Journal of Materials Chemistry C

ROYAL SOCIETY OF CHEMISTRY

REVIEW

View Article Online
View Journal | View Issue

Cite this: J. Mater. Chem. C, 2021, 9, 10557

Solid-solution (alloying) strategies in crystalline molecular conductors

Marc Fourmigué

Received 10th May 2021,
Accepted 16th June 2021

DOI: 10.1039/d1tc02160e

rsc.li/materials-c

In this review, we describe solid solution strategies employed in molecular conductors, where the control of their transport and magnetic properties (metallic or superconducting behavior, metal–insulator transitions, *etc.*) is the main goal. We first describe the main features of molecular conductors in order to identify which molecular entities are prone to be substituted by others in solid solutions, to which extent and for what purpose. We then describe the different crystal growth techniques used toward solid solution preparation and the nature of the molecular species, whether electroactive or not, which have been used, in cation or anion radical salts, in charge transfer salts and in single component conductors, in more than sixty reported examples. Topics such as preferential insertion and miscibility, the nature of disorder and the different analytical tools used for characterizing these alloys are presented. The consequences of alloying on conductivity and on phase transitions (superconductivity, anion ordering, Peierls transition, spin-Peierls transition), and the concepts of chemical pressure effects, band filling manipulation, and π–d interactions with magnetic anions are also discussed.

1 Introduction

Engineering crystal properties through solid solutions offers an opportunity to fine-tune the structural and physico-chemical properties of molecular materials, with, in some cases, the appearance of novel, unexpected behaviors. As stated by Lusi,[1] a plethora of terms has been used over the years to define what we called indiscriminately solid solutions or alloys. They can be defined as multi-component phases for which the component ratios can be varied in continuum. They differ in that respect from salts or co-crystals where the stoichiometry defines the exact composition expressed by integer ratios (1 : 2, 1 : 3, 1 : 2 : 1, *etc.*).[2] Solid solutions therefore have high potential for tuning molecular properties in a smooth and controlled way, over a broad range of compositions. Working with molecular solid solutions also induces notable differences in well-known inorganic alloys such as steel (Fe + C), brass (Zn + Cu), and binary (Si_xGe_{1-x}) and ternary ($In_xGa_{1-x}As$) semiconductors built out of atomic constituents which are held by strong covalent bonds.[3] Interactions between molecules in molecular solids are usually much weaker and the molecular entities maintain their integrity in the solid. Note, however, that in organic conductors, metallic bonding can play an important role in controlling the overall solid-state arrangement. In the following, we will restrict ourselves to crystalline, single-phase materials and will not consider molecular amorphous blends as used, for example, in molecular semiconductors,[3] or crystals grown on crystals through stepwise 3D epitaxial growth.[4]

The more general question of the effect of disorder in molecular alloys has been addressed from a thermodynamic point of view in relation with the effect of an increased entropy.[5] Several entropic effects can be considered in molecular crystals: configurational entropy, vibrational entropy and rotational entropy. Configurational entropy can be found because of

Univ Rennes, CNRS, ISCR (Institut des Sciences Chimiques de Rennes), UMR 6226, Campus de Beaulieu, 35000 Rennes, France. E-mail: marc.fourmigue@univ-rennes1.fr

Marc Fourmigué

Marc Fourmigué started his career in the Laboratoire de Physique des Solides (LPS) in Orsay, moving in 1995 to IMN in Nantes, and in 2002 to Angers. He joined the Institut des Sciences Chimiques de Rennes (ISCR) in 2006 and has been its director since 2017. As a molecular solid state chemist, he has developed a variety of radical species and their controlled crystallization (electrocrystallization) toward crystalline molecular conductors, molecular metals and magnetic materials. His activities have evolved towards the study of noncovalent intermolecular interactions in a crystal engineering approach, particularly σ-hole interactions in electro-active systems.

molecular disorder (one molecule or a part of a molecule disordered at two or more sites), eventually associated with temperature-dependent molecular motions and thermal expansion behaviors.[6] In solid solutions of molecular compounds, the nature of disorder (*vs.* clustering or spinodal decomposition) can play an important role, as shown recently in $CH_3NH_3PbI_3/CH_3NH_3PbBr_3$ alloys of hybrid halide perovskite semiconductors used for photovoltaic applications.[7] Furthermore, in addition to static substitutional disorder that arises from molecular substitution, orientational disorder at a given site can also play a role, with two isomorphous molecules or ions adopting different orientations.[8] Another difficulty one can encounter is the situation where co-crystallization of similar molecules does not, as previously believed, necessarily result in the formation of macroscopic crystals with the same homogeneous distribution of components.[9] This effect, observed in $[M_xM'_{1-x}(bipy)_3](PF_6)_2$ (M, M′ = Ni^{2+}, Fe^{2+}, Ru^{2+}; bipy: 2,2′-bipyridine) solid solutions, gives rise to crystals from the same batch with the composition varying notably (by as much as 15%) from the averaged composition. This effect described as supramolecular selectivity is explained by molecular recognition processes that lead to the partially selective aggregation of like molecules. These illustrate how difficult the full characterization of molecular solid solutions can be. For most reported examples detailed below, many of these questions about the nature of the disorder, the exact composition and structure of the crystals, and their homogeneity, were never addressed, limiting to some extent the conclusions that many authors draw on the correlation between alloy composition and physical properties.

In molecular materials, solid solution strategies are used extensively to control their different properties, such as magnetic, luminescence, and catalytic properties. The molecular magnetism community makes extensive use of alloying strategies. This is particularly true in coordination complexes exhibiting spin crossover (SCO) behavior. Substitution of counterions (for example, PF_6^- *vs.* AsF_6^-) or ligands or dilution of the magnetic center with other cations can have very important consequences on the cooperativity of the SCO and the eventual presence of structural phase transitions.[10–12] Another striking example involves the modulation of the Single Molecule Magnet (SMM) properties of pentadecanuclear cyanide-bridged clusters formulated as $\{Fe_{9-x}Co_x[W(CN)_8]_6(MeOH)_{24}\}$, where different Co/Fe metal ratios favor either $^{HS}Fe^{II}W^{V} \leftrightarrow {}^{HS}Fe^{III}W^{IV}$ charge transfer transition or slow magnetic relaxation effects.[13] Luminescent species, particularly those based on rare-earth complexes, offer another playing field for alloying strategies. For example, lanthanide complexes of the 5-methoxyisophthalate (mip^{2-}) ligand, formulated as $[Ln_2(mip)_3(H_2O)_8{\cdot}4H_2O]$, are prepared with a mixture of up to six different lanthanide ions (Nd^{3+}, Sm^{3+}, Eu^{3+}, Gd^{3+}, Tb^{3+}, Dy^{3+}). At a unique irradiation wavelength (λ_{exc} = 325 nm), these compounds exhibit almost 20 emission peaks in both the visible and NIR regions at RT, an unprecedented richness of the emission spectrum of great interest as far as luminescent barcodes are concerned.[14] The chemistry of metal organic frameworks (MOFs) also provides several examples of successful alloying strategies as those reported (i) to tune catalytic properties through the In^{3+}/Ga^{3+} metal ion ratio,[15] or (ii) to manipulate the mechanical and dynamical properties of formate-based perovskites in the $[NH_3NH_2]_{1-x}[NH_3OH]_xZn(HCOO)_3$ series.[16]

In this review, we will focus on solid solution strategies employed in molecular conductors, where the control of the transport properties (metallic or superconducting behavior, metal–insulator transitions with associated magnetic properties) is the main goal. To do so, it is important to first describe the main features of molecular conductors in order to identify which molecular entities are prone to be substituted by others in solid solutions and for what purpose.

The term "molecular conductors" encompasses, in this review, a broad range of crystalline materials built out of molecular entities, be they of organic or of coordination chemistry origin, able to generate charge carriers. Intermolecular interactions in the solid state, most often of 1D or 2D nature, favor the formation of bands, with a limited gap in semiconducting systems ($\approx 10^{-4}$ S cm^{-1} < σ_{RT} < $\approx$1 S cm^{-1}), and a limited bandwidth in gapless metallic systems (σ_{RT} > $\approx$1 S cm^{-1}). These characteristics are the consequences of strong electronic correlations between charge carriers,[17] and offer a wide variety of ground states and phase transitions, referred to as charge density waves (CDWs), spin density waves (SDWs), Peierls transition, spin-Peierls (SP) transition, dimer-Mott (DM) insulating phase, Mott-insulator states, charge-order (CO), superconductivity, *etc.*[18] From a composition point of view, we can distinguish three main different classes of compounds, each of them amenable to different solid solution strategies.

Charge-transfer salts are based on the association of two different electroactive molecules: one is referred to as the electron donor (D) and the other is referred to as the electron acceptor (A). Upon co-crystallization from solution or co-sublimation, a D·A co-crystal is formed and its electronic nature varies with the $E^{1/2}$ redox potentials of both D and A molecules.[19] In solution, electron transfer can normally occur if $E_{red}(A) > E_{ox}(D)$. Since the formation of a crystalline solid favors ionic phases, electron transfer in D·A co-crystals can be observed already if $E_{red}(A) - E_{ox}(D) > -(0.25–035)$ V. A partial degree of charge transfer, $0 < \rho < 1$, is found in segregated structures with DDD and AAA stacks, as in $TTF^{+\rho}{\cdot}TCNQ^{-\rho}$ (Scheme 1),[20] where the Fermi level crosses both the HOMO band of D and the LUMO band of A, at the origin of the metallic character. Solid solutions can be considered within such charge-transfer salts by replacing either D or A with an isomorphous molecule, *i.e.* $(D_xD'_{1-x})$·A or $D{\cdot}(A_xA'_{1-x})$.

Ion-radical salts are based on one single electroactive molecule (either D or A), respectively, oxidized or reduced in the radical cation $D^{+\bullet}$ or radical anion $A^{-\bullet}$ form. Partial charge transfer is also possible, for example with the recurrent 2 : 1 stoichiometry in $(D)_2{\cdot}X$ (ρ = 0.5 if X is a monovalent anion). More complex situations are found in systems like $(D)_3{\cdot}X_2$ or with non-stoichiometric band filling,[21] as in TTF halides $(TTF)X_x$ (x = 0.77–0.80 with Cl^-, x = 0.71–076 with Br^- and x = 0.70–0.72 for I^-).[22] The Fabre salts (2 : 1 salts built out of TMTTF molecules), the Bechgaard salts (2 : 1 salts built out of TMTSF molecules),[18] and the large family of BEDT-TTF salts[23] (and BETS and BET analogs)[24,25] belong to this class of molecular conductors. Solid solutions here can take on

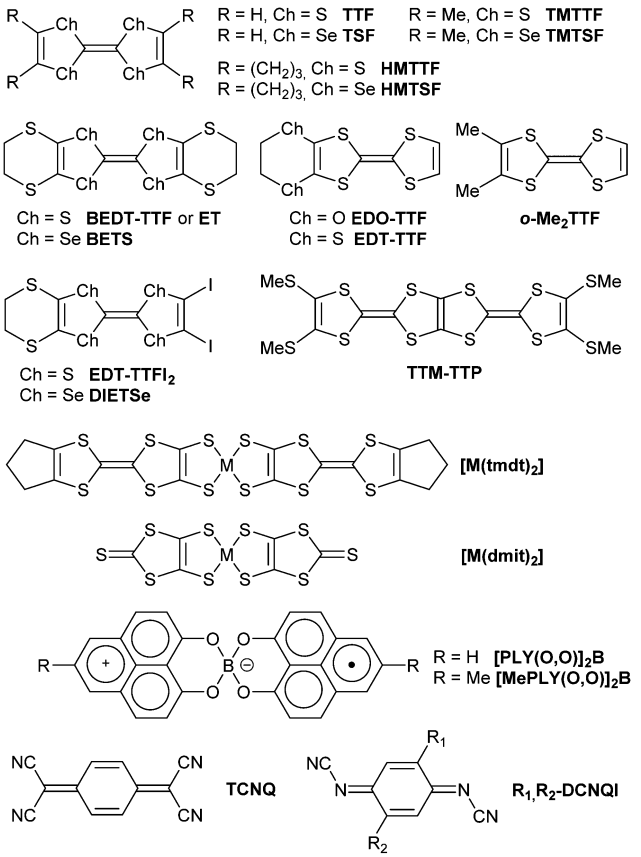

Scheme 1 Electroactive molecules involved in solid solutions.

different aspects, by replacing the electroactive molecule with an isomorphous one as in charge-transfer salts, *i.e.* $(D_xD'_{1-x})_nX$, or by replacing the counter-ion with an isomorphous one, *i.e.* $D_n(X_xY_{1-x})$. If X and Y differ in charge, band filling will also be impacted, a difficult but sought-after goal, as we will see in the following.

Single component conductors are built from one single molecular species, be it radical in nature or not. Among the organic radical species, we can mention spiro-bis(phenalenyl)boron radicals,[26] dithiadiazolyl[27] or dithiazolyl radicals,[28] and hydrogen-bonded TTF dimers.[29,30] Among the coordination complexes, the most famous series is based on neutral tetrathiafulvalene dithiolate complexes such as $[M(tmdt)_2]$,[31] while neutral radical gold complexes such as $[Au(R\text{-thiazdt})_2]^\bullet$ have emerged as an attractive family.[32] In-between we can find neutral nickel bis(dithiolene) complexes whose semiconducting behavior can be changed into a metallic one under application of high pressures.[33] Among all these single-component conductors, alloying strategies have been considered up to now only upon metal substitution, in spiro-bis(phenalenyl)boron radicals (B *vs.* Be) and in TTF–dithiolate complexes (M = Ni, Pd, Pt *vs.* Cu, Au).

Reported solid solutions of molecular conductors analyzed in this Review are gathered in Tables 1 and 2, distinguishing those involving alloys based on electroactive molecules (Table 1) and those involving alloys based on counter-ions (Table 2).

2. Chemical properties of solid solutions in molecular conductors

In the following, we will describe the different methods used for the preparation of solid solutions of molecular conductors, together with the analytical methods used to particularly characterize their composition. We will also address important issues about the nature of the mixed species (volume, shape, charge, spin, *etc.*).

2.1 Crystal growth methods

Crystalline molecular conductors are essentially obtained through two different methods both involving an electron transfer, either crystallization from solution using an oxidant or a reducing agent (eventually inserted itself in the structure), or electrocrystallization where the electron transfer performed at the electrode is followed by the precipitation (crystallization) of the conducting salts on the electrode itself.

2.1.1 Cocrystallization. This first approach is illustrated using the well-known TTF·TCNQ conductor. Its extension to solid solutions with the selenated analog, *i.e.* tetraselenafulvalene (TSF), was reported in 1977 for $(TSF)_x(TTF)_{1-x}(TCNQ)$,[34] obtained either by slow diffusion of the constituents together[35] or by cooling from saturated solutions, with x varying continuously between 0 and 1. On the other hand, the solid solution $(HMTTF)_x(HMTSF)_{1-x}$·TCNQ could be prepared only with a small HMTTF content ($x = 0.05$) despite a 25 : 75 HMTTF/HMTSF ratio in solution, an indication of the probably much lower solubility of the selenated phase.[37]

Reducing agents such as TDAE [tetrakis(dimethylamino)-ethylene] are used for the preparation of $TDAE{\cdot}(C_{60})_{1-x}(C_{70})_x$ alloys, which precipitate rapidly from solutions of C_{60} and C_{70} in a benzene/toluene mixture.[64] TDAE was also used a reducing agent without insertion into the crystal in the single-component conductor derived by the reduction of the spiro-bis(9-oxido-phenalenone)boron cation denoted $[PLY(O,O)]_2B^+$.[53] Co-crystallization of solutions of this cation with selected amounts of the neutral beryllium analog $[PLY(O,O)]_2Be$ in the presence of TDAE leads to the formation of a series of solid-state solutions with the composition $[PLY\text{-}(O,O)]_2B_{1-x}Be_x$. The crystallization process is driven by the insolubility of the radical $[PLY(O,O)]_2B$, which apparently induces the co-crystallization of $[PLY(O,O)]_2Be$ with x values not exceeding 0.2. Higher Be concentrations are reached in the methyl-substituted analogs with x values up to 0.59.[54]

Reduction processes are also involved in the preparation of solid solutions of the DCNQI acceptor and analogs. As reported by Hünig *et al.*, mixing two (or even three) different DCNQIs in the presence of $CuBr_2$ and copper wire afforded crystallization of 26 binary alloys such as $[(Me_2)_{1-x}(MeBr)_xDCNQI]_2Cu$, and even one ternary alloy.[61] Under these conditions, the different reduction potentials of two DCNQIs do not affect the composition of the salt and the most reducible acceptor was not inserted preferentially. Solid solutions involving Me_2DCNQI and for example its deuterated analog $Me_2DCNQI\text{-}d_8$ were also prepared upon reaction of the acceptor molecules with Bu_4NI as a reductant in the presence of a copper salt, namely

Table 1 Reported solid solutions of molecular conductors based on different electroactive donor or acceptor molecules

Compound	Pairs of alloyed molecules or ions	Composition	Ref.
Charge-transfer salts			
$(TSF)_x(TTF)_{1-x}(TCNQ)$	TTF, TSF	$0 \leq x \leq 1$	34–36
$(HMTSF)_{1-x}(HMTTF)_xTCNQ$	HMTTF, HMTSF	0.05	37
$(NMP)_x(Phen)_{1-x}TCNQ$	NMP, Phen	$0.5 \leq x \leq 1$	38 and 39
Cation-radical salts			
$[(TMTSF)_{1-x}(TMTTF)_x]_2ClO_4$	TMTTF, TMTSF	$0 \leq x \leq 0.30$	40
$[(TMTSF)_{1-x}(TMTTF)_x]_2ReO_4$	TMTTF, TMTSF	$0 \leq x \leq 1$	41 and 42
$[(TMTSF)_{1-x}(TMTTF)_x]_2PF_6$	TMTTF, TMTSF	$x < 0.25$, 0.85	43
κ-$[(ET)_{1-x}(BEDT\text{-}STF)_x]_2$, $Cu[N(CN)_2]Br$	BEDT-TTF, BEDT-STF	$0 \leq x \leq 1$	44
κ-$[(ET)_{1-x}(BEDSeT\text{-}TTF)_x]_2$, $Cu[N(CN)_2]Br$	BEDT-TTF, BEDSeT-TTF	$0 \leq x \leq 0.26$	45
$[(EDO\text{-}TTF)_{1-x}(MeEDO\text{-}TTF)_x]_2PF_6$	EDO-TTF, MeEDO-TTF	$x < 0.6$, $0.9 < x$	46
$(Perylene)_2[Au_{1-x}Pt_x(mnt)_2]$	Au^{3+}, Pt^{2+}	$0 \leq x \leq 0.50$	47–49
Single component conductors			
$[NiOC_4]_{1-x}[AuOC_4]_x$	Ni^{2+}, Au^{3+}	$0 \leq x \leq 1$	50
$[Ni_{1-x}Au_x(tmdt)_2]$	Ni^{2+}, Au^{3+}	$0 \leq x \leq 1$	51
$[Ni_{1-x}Cu_x(tmdt)_2]$	Ni^{2+}, Cu^{2+}	$x \leq 0.27$	52
$[PLY(O,O)]_2B_{1-x}Be_x$	B^{3+}, Be^{2+}	$0 \leq x \leq 0.2$	53
$[MePLY(O,O)]_2B_{1-x}Be_x$	B^{3+}, Be^{2+}	$0 \leq x \leq 0.59$	54
Anion-radical salts			
$[Cl\text{-}BzPy][Ni_xPt_{1-x}(mnt)_2]$	Ni^{2+}, Pt^{2+}	$0 \leq x \leq 1$	55
$[NO_2\text{-}BzPy][Ni_xAu_{1-x}(mnt)_2]$	Ni^{2+}, Au^{2+}	$0 \leq x \leq 1$	56
$(Me_4N)[Ni_xPd_{1-x}(dmit)_2]_2$	Ni^{2+}, Pd^{2+}		57
$[(Me_2DCNQI)_{1-x}(Me_2DCNQI\text{-}d_8)_x]_2Cu$	Me_2DCNQI, $Me_2DCNQI\text{-}d_8$	$0 \leq x \leq 1$	58 and 61
$[(Me_2)_{1-x}(MeBr)_xDCNQI]_2Cu$	Me_2DCNQI, MeBrDCNQI	$0 \leq x \leq 1$	59–61
$[(Me_2)_{1-x}(MeCl)_xDCNQI]_2Cu$	Me_2DCNQI, MeClDCNQI	0.75	62
$[(Me_2)_{1-x}(MeI)_xDCNQI]_2Cu$	Me_2DCNQI, MeIDCNQI	0.70	61 and 62
$[(MeCl)_{1-x}(MeBr)_xDCNQI]_2Cu$	MeClDCNQI, MeBrDCNQI	0.60	62
$[(MeBr)_{1-x}(MeI)_xDCNQI]_2Cu$	MeBrDCNQI, MeIDCNQI	$0 \leq x \leq 1$	61 and 62
$[(MeCl)_{1-x}(MeI)_xDCNQI]_2Cu$	MeClDCNQI, MeIDCNQI	0.25	62
$K_3(C_{60})_{1-x}(C_{70})_x$	C_{60}, C_{70}	$x \leq 0.5$	63
$TDAE{\cdot}(C_{60})_{1-x}(C_{70})_x$	C_{60}, C_{70}	$0 \leq x \leq 0.5$	64

$(Et_4N)_2CuBr_4$.[58] These DCNQI salts can also be prepared by electrocrystallization (see below).[59,60]

Chemical oxidation processes have also been used in the crystallization of solid solutions of $[Pd(dmit)_2]$ dithiolene complexes, such as $(Me_4Sb)_{1-x}(EtMe_3Sb)_x[Pd(dmit)_2]_2$ and $(Et_2Me_2Sb)_{1-x}$-$(EtMe_3Sb)_x[Pd(dmit)_2]_2$.[67] They are prepared indeed through the slow air oxidation of $[Pd(dmit)_2]^{2-}$ ions in the presence of the corresponding cations (Me_4Sb^+ *vs.* $EtMe_3Sb^+$ and $Et_2Me_2Sb^+$ *vs.* $EtMe_3Sb^+$) and acetic acid. This method proved to be very suitable for the preparation of large and high-quality alloyed crystals.

2.1.2 Electrocrystallization. Electrocrystallization is by far the most general method used for the preparation of molecular conductors.[100] This method for preparing solid solutions containing two different electroactive species (Table 1) is based on their mixing in the anodic (for donor molecules) or the cathodic (for acceptor molecules) compartment of an electrocrystallization cell, in the presence of the chosen electrolyte dissolved in both compartments. A constant current intensity is usually applied for several days/weeks. The main series of alloys explored so far are the Fabre/Bechgaard salts where mixing of TMTTF and TMTSF was performed in their 2:1 salts with ClO_4^-,[40] ReO_4^-,[41] and PF_6^-.[43] Indeed both TMTTF and TMTSF salts exhibit closely related structures and can be described using a unique (p,T) phase diagram.[18] Considering that both molecules do not oxidize at the same potential, the PF_6^- alloy $[(TMTSF)_{1-x}(TMTTF)_x]_2PF_6$ was originally prepared in a potentiostatic mode at 0.25–0.30 V, *i.e.* below the oxidation potential of both donor molecules (TMTTF: +0.26 V; TMTSF: +0.43 V).[43] A slightly different strategy was used for the ClO_4^- alloy prepared at a higher intermediate potential value (0.4 V).[40] The lower solubility of the TMTSF salts limited, however, the insertion of TMTTF to a maximum value of x = 0.30 in $[(TMTSF)_{1-x}(TMTTF)_x]_2ClO_4$, and of x = 0.25 in $[(TMTSF)_{1-x}(TMTTF)_x]_2PF_6$. These problems were not found for the ReO_4^- salt, *i.e.* $[(TMTSF)_{1-x}(TMTTF)_x]_2ReO_4$,[41] where galvanostatic methods associated with smaller current densities and hence a slower crystallization process afforded three alloys with $x \approx 0.2$, 0.55 and 0.8. The well-known κ-$(ET)_2Cu[N(CN)_2]Br$ kappa-Br phase has also been the subject of alloying strategies involving as second donor molecules BEDT-STF or BEDSe-TTF.[44,45] Finally, dithiolene complexes offer another series where solid solutions can be easily prepared by electrocrystallization of two different complexes differing only by the nature of the central metal, as in the isoelectronic series based on Ni/Pd/Pt complexes. Besides, solid solutions mixing group 10 (Ni, Pd, Pt) and group 11 (Cu, Au) metal complexes lead to a modification of the overall electron count and hence of the band filling.[47–57]

Electrocrystallization is the synthetic method of choice for the elaboration of solid solutions involving two different counter-ions with analogous symmetry, shape and charge: for example, ClO_4^- *vs.* ReO_4^-. Numerous examples have been reported and some are collected in Table 2. In most cases, the whole composition range can be explored. Also, because the electrolytes

Table 2 Reported solid solutions of molecular conductors based on different counter-ions

Compound	Mixed counter-ions	Composition	Ref.
Anion radical salts			
$(Me_2DCNQI)_2Li_{1-x}Cu_x$	Li^+, $Cu^{+,2+}$	$0 \leq x \leq 1$	65 and 66
$(Me_4Sb)_{1-x}(EtMe_3Sb)_x[Pd(dmit)_2]_2$	Me_4Sb^+, $EtMe_3Sb^+$	$0 \leq x \leq 1$	67
$(Et_2Me_2Sb)_{1-x}(EtMe_3Sb)_x[Pd(dmit)_2]_2$	$Et_2Me_2Sb^+$, $EtMe_3Sb^+$	$0 \leq x \leq 1$	67
Cation-radical salts			
$(o\text{-DMTTF})_2Br_xCl_{1-x}$	Br^-, Cl^-	$0 \leq x \leq 1$	68
$(o\text{-DMTTF})_2Br_xI_{1-x}$	Br^-, I^-	$0 \leq x \leq 1$	68
$(TMTSF)_2(ClO_4)_{1-x}(ReO_4)_x$	ClO_4^-, ReO_4^-	$x < 0.17$	69–72
$(TMTSF)_2(AsF_6)_{1-x}(FeCl_4)_x$	AsF_6^-, $FeCl_4^-$	10^{-3}	73
$(TMTTF)_2(SbF_6)_{1-x}(AsF_6)_x$	AsF_6^-, SbF_6^-	$0 \leq x \leq 1$	74 and 75
$(TMTSF)_2(TaF_6)_{1-x}(PF_6)_x$	TaF_6^-, PF_6^-	$0 \leq x \leq 1$	76
$\delta m\text{-}(ET)_2(TaF_6)_{1-x}(PF_6)_x$	TaF_6^-, PF_6^-	0.06	76
$\delta o\text{-}(ET)_2(TaF_6)_{1-x}(PF_6)_x$	TaF_6^-, PF_6^-	0.57	76
$\beta\text{-}(ET)_2(I_3)_{1-x}(IBr_2)_x$	IBr_2^-, I_3^-	$0 \leq x \leq 1$	77 and 78
$\beta\text{-}(ET)_2(IBr_2)_{1-x}(I_2Br)_x$	IBr_2^-, I_2Br^-	$0 \leq x \leq 1$	77 and 78
$\beta\text{-}(ET)_2(I_2Br)_{1-x}(I_3)_x$	I_2Br^-, I_3^-	$0 \leq x \leq 1$	77 and 78
$\beta\text{-}(ET)_2(I_3)_{1-x}(AuI_2)_x$	AuI_2^-, I_3^-	0.1, 0.26, 0.9	79 and 80
$\theta\text{-}(ET)_2(I_3)_{1-x}(AuI_2)_x$	AuI_2^-, I_3^-	<0.02	81
$(ET)_4[Ni(CN)_4]_x[Pt(CN)_4]_{1-x}$	$[Ni(CN)_4]^{2-}$, $Pt(CN)_4]^{2-}$	≈ 0.5, 0.14	82
$\kappa\text{-}(ET)_2Cu[N(CN)_2]Br_xCl_{1-x}$	Cl^-, Br^-	$0 \leq x \leq 1$	83–85
$\theta\text{-}(ET)_2(Rb_{1-x}Cs_x)Zn(SCN)_4$	Rb^+, Cs^+	$0 \leq x \leq 1$	86
$\lambda\text{-}(ET)_2(GaCl_4)_{1-x}(CoCl_4)_x$	$GaCl_4^-$, $CoCl_4^{2-}$	$0 \leq x \leq 0.06$	87
$\delta'\text{-}(ET)_2(GaCl_4)_{1-x}(CoCl_4)_x$	$GaCl_4^-$, $CoCl_4^{2-}$	0.05, 0.14	87
$\alpha\text{-}(ET)_3(CoCl_4)_{1-x}(GaCl_4)_x(TCE)$	$GaCl_4^-$, $CoCl_4^{2-}$	0.54, 0.57, 0.62	87
$\beta'\text{-}(ET)_3(CoCl_4)_{1-x}(GaCl_4)_x$	$GaCl_4^-$, $CoCl_4^{2-}$	0.88, 0.66	87
$\beta''\text{-}(ET)_2(SF_5RSO_3)_{1-x}(SF_5R'SO_3)_x$	R,R′ = CH_2CF_2, CHF	$0 \leq x \leq 1$	88
$\beta''\text{-}(ET)_2(SF_5RSO_3)_{1-x}(SF_5R'SO_3)_x$	R,R′ = CH_2–CF_2, CHFCF	$0 \leq x \leq 1$	88
$\lambda\text{-}(BETS)_2GaBr_xCl_{4-x}$	$(GaBr_xCl_{4-x})^-$ (x = 1–4)		89 and 90
$\lambda\text{-}(BETS)_2GaF_xCl_{4-x}$	$(GaF_xCl_{4-x})^-$ (x = 1–4)		91
$\lambda\text{-}(BETS)_2Fe_xGa_{1-x}Cl_4$	$FeCl_4^-$, $GaCl_4^-$	0.43, 0.55	92–94
$(DIETSe)_2GaBr_xCl_{4-x}$	$(GaBr_xCl_{4-x})^-$ (x = 1–4)		95
$(DIETSe)_2FeBr_xCl_{4-x}$	$(FeBr_xCl_{4-x})^-$ (x = 1–4)		95
$(TTM\text{-}TTP)FeBr_xCl_{4-x}$	$(FeBr_xCl_{4-x})^-$ (x = 1–4)		96
$(TTM\text{-}TTP)GaBr_xCl_{4-x}$	$(GaBr_xCl_{4-x})^-$ (x = 1–4)		97
$(TTM\text{-}TTP)Fe_{1-x}Ga_xCl_4$	$FeCl_4^-$, $GaCl_4^-$	0.1	97
$(TTM\text{-}TTP)Fe_{1-x}Co_xCl_4$	$FeCl_4^-$, $CoCl_4^{2-}$	0.05, 0.40	98
$(TTM\text{-}TTP)Ga_{1-x}Co_xCl_4$	$GaCl_4^-$, $CoCl_4^{2-}$	0.30	98
$(TTM\text{-}TTP)Mn_{1-x}Co_xCl_4$	$MnCl_4^{2-}$, $CoCl_4^{2-}$	0.90	98
$\beta\text{-}(EDT\text{-}TTF\text{-}I_2)_2[Pb_{2/3+x}Ag_{1/3-2x}\square_xI_2]_3$	Pb^{2+}, Ag^+	0.05	99

are used in large excess compared to the electroactive species, very small x values can be investigated when doping effects are considered rather than exploration of the whole $0 \leq x \leq 1$ range. Electrocrystallization conditions might require a difficult optimization in order to be able to isolate solid solutions with a broad composition range. For example, in the series of $\beta\text{-}(ET)_2(X1)_{1-x}(X2)_x$ alloys (X1, X2 = I_3^-, I_2Br^-, IBr_2^-),[78] mixed crystals having a wide composition range of anions were obtained from only nitrobenzene for X1 = IBr_2^- and X2 = I_3^-, from only chlorobenzene for X = I_2Br^- and X2 = I_3^-, and from only THF for X1 = I_2Br^- and X2 = IBr_2^-, and crystals having such a wide composition range of anions were not obtained from other organic solvents. Note that the electrocrystallization itself can generate two different anions, as reported upon crystal growth of $\beta\text{-}(BEDT\text{-}TTF)_2AuI_2$ in the presence of solely Bu_4NAuI_2. When performed at high potentials, it afforded the solid solution $\beta\text{-}(BEDT\text{-}TTF)_2[(AuI_2)_{0.26}(I_3)_{0.74}]$, a probable consequence of the oxidation and decomposition of the $Au^II_2^-$ anion.[80]

2.2 Nature of the components of a molecular alloy

Engineering molecular solid solutions is not always a straightforward task.[101] It is essentially based on the assumption that the similarity of size and shape is sufficient, although the intermolecular interactions between molecules in the crystal also play an important role.[102] In that respect, the examples reported in Tables 1 and 2 are not so numerous and often limited to very similar systems.

Perhaps the most identical, yet different molecules to be alloyed are those with different isotopes (H *vs.* D, ^{13}C, ^{34}S, ^{77}Se). In the field of molecular conductors, isotope introduction has been originally performed in order to observe any change in T_c, *i.e.* the ''isotope effect'' in superconducting salts.[103] Besides, solid state NMR is an important tool for investigating the magnetic and conducting properties of such systems in order to estimate the density of states from the Knight-shift and the spin–lattice relaxation rate. It requires a ^{13}C enrichment of the molecules, most often on the two central carbon atoms of the TMTTF,[104] TMTSF or BEDT-TTF molecules.[105] With this enrichment, spectral splitting occurs because of the resulting coupled spin system and induces a so-called Pake doublet.[106] To avoid this problem, ^{13}C-enriched TMTTF and ET molecules were prepared from a mixture of labelled and unlabelled dithiole precursors, affording a mixture with 10% ^{13}C-TMTTF

in unlabelled TMTTF,[104] and that containing less than 7% $^{13}C{=}{=}^{13}C$ double side-enriched ET in a major ^{13}C-single side-enriched ET molecule respectively.[105] These mixtures were electro-crystallized to yield solid solutions composed of double side-enriched, single side-enriched and non-enriched donor molecules.

Another series where isotopic substitution proved to be particularly fruitfull is based on the Me_2DCNQI acceptor, also known as its fully deuterated analog, $Me_2DCNQI\text{-}d_8$.[58] Indeed, the slightly smaller size of deuterium compared to hydrogen makes deuteration of molecules a very useful tool for tentatively paralleling the effect of an external pressure, as also explored in this area with BEDT-TTF-d_8.[107]

As shown in Scheme 2a, the donor molecules used in alloys of cation radical salts are essentially based on a S/Se substitution, on the central TTF core as well as on side substituents. One single example involves the introduction of an extra methyl group in $[(EDO\text{-}TTF)_{1-x}(MeEDO\text{-}TTF)_x]_2PF_6$ alloys but the whole composition range could not be prepared except for $x < 0.6$ and $x > 0.9$.[46] A much broader choice was offered in the $(DCNQI)_2Cu$ salts where many acceptors with different substituents in the 2 and 5 positions could be mixed (Scheme 2b).

Most common solid solutions involve two different counter-ions with analogous symmetry, shape and charge: for example, Cl^- *vs.* Br^- *vs.* I^-, ClO_4^- *vs.* ReO_4^-, PF_6^- *vs.* AsF_6^- *vs.* SbF_6^-, $FeCl_4^-$ *vs.* $GaCl_4^-$, and I_3^- *vs.* I_2Br^- *vs.* IBr_2^-, or in radical anion salts, Li^+ *vs.* Cu^+, all collected in Table 2. In most cases, the whole composition range can be explored.

Organic counter-ions offer an increased degree of complexity as reported in the alloys involving Me_4Sb^+ *vs.* $EtMe_3Sb^+$,[67] and $SF_5CH_2CF_2SO_3^-$ *vs.* $SF_5CHFSO_3^-$.[88] In these salts, to the positional disorder of the two species at a given crystallographic site for the counter-ion is added substitutional disorder even more difficult to characterize (see Section 2.4). A specific warning should be made here for reported solid solutions involving the $GaCl_4^-/GaBr_4^-$ and $FeCl_4^-/FeBr_4^-$ pairs. Indeed, several interesting phases with the BETS donor molecule have been reported, such as the organic superconductor λ-$(BETS)_2GaCl_4$ and the isostructural λ-$(BETS)_2FeCl_4$ which exhibits a sharp MI transition around 8 K. On the other hand, κ-type salts with various anions such as $GaC1_4^-$, $GaBr_4^-$, $FeCl_4^-$, $FeBr_4^-$, and $InC1_4^-$ exhibit metallic behavior down to 4 K.[24] Solid solutions of the λ-phases were investigated with, for example, $GaCl_4^-$ and $GaBr_4^-$ in a 1 : 3 ratio written as "$GaBrCl_3^-$".[89,90] It has been reported, however, that the halogen ions of mixed halide gallium anions tend to be easily substituted by other halogen ions in solution.[108] This scrambling in solution implies that the description "$GaBrC1_3^-$" does not represent just one species $GaBrC1_3^-$, but rather a complex mixture of $GaC1_4^-$, $GaBrCl_3^-$, $GaBr_2C1_2^-$, $GaBr_3Cl^-$, and $GaBr_4^-$. In the present example, the distribution was approximatively 5 : 6 : 3 : 1 : 0 and the Br/Cl distribution was different on the four crystallographically different halide sites. Similar scrambling reactions and added complexity are also reported in solid solution involving DIETS or TTM-TTP donor molecules with mixtures of $FeCl_4^-$ and $FeBr_4^-$ iron complexes.[95,96]

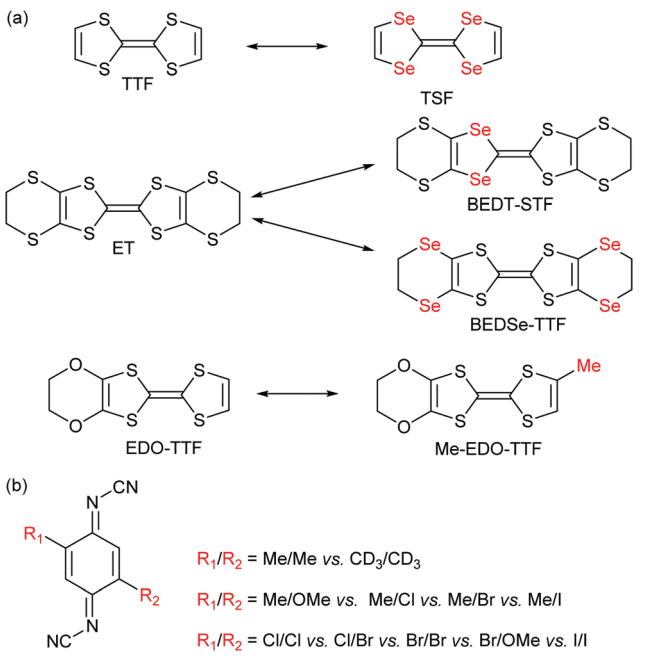

Scheme 2 (a) Examples of pairs of donor molecules investigated in alloys. (b) The different DCNQI acceptor molecules used in alloys.

2.3 Miscibility: doping, preferential insertion

In several situations where the two extreme structures differ too much from each other, a full miscibility of the two partners cannot be reached and the resulting salts are much better described as doped materials. These compositions are also of interest for highly sensitive properties such as superconductivity (see Section 3.4), upon insertion of disorder or of magnetic defects. For example, insertion of the tetrahedral and magnetic ($S = 5/2$) $FeCl_4^-$ anion into $(TMTSF)_2(AsF_6)$ was limited to an x value of 10^{-3} in the alloy formulated as $(TMTSF)_2(AsF_6)_{1-x}(FeCl_4)_x$, despite the 8 : 2 ratio of AsF_6^- : $FeCl_4^-$ in the electrolyte.[73] Such doped systems are also prepared on purpose for EPR investigations of paramagnetic dithiolene complexes diluted in diamagnetic matrices: for example, $[Ni(dt)_2]^-$ in diamagnetic $[Au(dt)_2]^-$[109] and $[Cu(dt)_2]^{2-}$ in diamagnetic $[Ni(dt)_2]^{2-}$.[110]

In most situations, however, the full range of compositions can be obtained but often with an x value in the crystal which differs from the nominal concentration in solution. Concerning the S/Se exchange in donor molecules, $(TSF)_x(TTF)_{1-x}(TCNQ)$ is the only example where a slight enrichment in TTF is observed over that of the initial solution composition.[34] Other examples go in the opposite direction, *i.e.* a systematic preferential insertion of the selenated molecule associated with a decreased solubility of the corresponding salt, as in $[(TMTSF)_{1-x}(TMTTF)_x]_2ClO_4$,[40a] $[(TMTSF)_{1-x}(TMTTF)_x]_2PF_6$,[43] $(HMTTF)_{0.05}(HMTSF)_{0.95}TCNQ$,[37] and κ-$[(ET)_{1-x}(BEDSeT\text{-}TTF)_x]_2Cu[N(CN)_2]Br$.[45] Similar strong effects are observed in radical-anion salts as the DCNQI alloys $[(Me_2)_{1-x}(MeBr)_xDCNQI]_2Cu$, where a 0.2 molar fraction of (MeBr)DCNQI in solution results in an $x = 0.7$ fraction in the solid.[59,60] Systematic studies related to these preferential insertion effects are scarce but give invaluable information about the

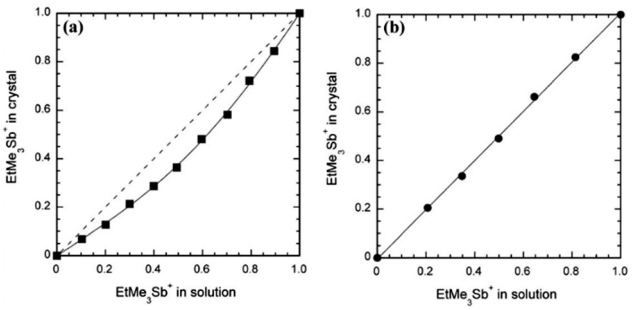

Fig. 1 Mole fraction of $EtMe_3Sb^+$ in the crystal (x) as a function of that in solution for (a) $(Me_4Sb)_{1-x}(EtMe_3Sb)_x[Pd(dmit)_2]_2$ and (b) $(Et_2Me_2Sb)_{1-x}$-$(EtMe_3Sb)_x[Pd(dmit)_2]_2$. Reproduced from ref. 67 with permission from Wiley-VCH.

relative stability/solubility of two different compounds differing only by the counterion. In that respect we can mention, for example, the mixed-valence 1 : 2 salts of the electroactive $[Pd(dmit)_2]$ with Me_4Sb^+, $EtMe_3Sb^+$ or $Et_2Me_2Sb^+$ cations.[67] As shown in Fig. 1, the molar fraction of the bulkier/disordered $EtMe_3Sb^+$ cation in crystalline solid solutions with Me_4Sb^+ is systematically smaller than that in the electro-crystallized solution, showing a more "favorable" crystal growth with the more compact Me_4Sb^+ cation. On the other hand, introduction of the even bulkier $Et_2Me_2Sb^+$ cation in competition with $EtMe_3Sb^+$ (Fig. 1b) shows no sign of discrimination, a consequence of the similar steric constraints brought by the two ethyl-containing cations. Indeed, in the pristine $EtMe_3Sb^+$ salt, the $EtMe_3Sb^+$ cation is located on a two-fold axis and exhibits disorder with two possible orientations, giving an overlapped image with an apparent $Et_2Me_2Sb^+$ cation with 50% occupancy of the ethyl groups.

A very different situation is observed in 2 : 1 cation radical salts of *o*-Me_2TTF with Cl^-, Br^- and I^- anions.[68] In this original quadratic structure, the halide is embedded in a set of weak C–H···X^- hydrogen bonds. Solid solutions were reported involving either Cl^-/Br^- or Br^-/I^- pairs. As shown in Fig. 2, preferential insertion is observed here with the Br^- anion, in solid solutions with either Cl^- or I^-, demonstrating that the most "stable" structure, or the best compromise between size and all intermolecular interactions, is reached with the intermediate-size Br^- anion. Note that the authors reported that this bromide

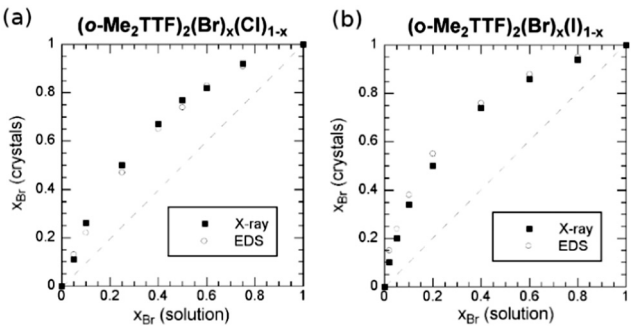

Fig. 2 Mole fraction (x) of the Br^- anion in the crystals, as a function of that in solution for (a) $(o\text{-}Me_2TTF)_2(Br)_x(Cl)_{1-x}$ and (b) $(o\text{-}Me_2TTF)_2(Br)_x(I)_{1-x}$. Reproduced from ref. 68 with permission from Wiley-VCH.

phase actually gives the largest crystals during the electro-crystallization experiments.

More complex anions can also have similar effects, as reported in θ-$(BEDT\text{-}TTF)_2(Rb_{1-x}Cs_x)Zn(SCN)_4$ with preferential insertion of Cs^+ over Rb^+,[86] or in κ-$(BEDT\text{-}TTF)_2Cu[N(CN)_2]Br_xCl_{1-x}$ salts with preferential insertion of the Br^- ion.[83]

2.4 Disorder evaluation

In essentially all reported examples, the statistical mixing of two partners in solid solutions is taken for granted. This was investigated in one single example by X-ray diffraction at low temperatures ($T < 30$ K) where the diffuse scattering due to thermal vibrations is negligible, in comparison with the effects of intrinsic substitutional disorder. In $TMTSF_2(ReO_4)_{1-x}(ClO_4)_x$ solid solutions,[71] the intense diffuse scattering observed near the origin of the reciprocal space was shown to decrease with increasing Bragg (θ) angle. This θ dependence follows, at all concentrations, the monotonic Laue scattering associated with random disorder which can be written as:

$$I(\theta) = Cx(1 - x)[f_A(\theta) - f_B(\theta)]^2$$

where f_A and f_B are the form factors of the ReO_4^- and ClO_4^- anions and C is a scale factor. Since (i) the anions' orientations are similar in both pure salts and (ii) the Re–O and Cl–O distances are also comparable, it was confidently concluded that the ReO_4^-/ClO_4^- substitutional disorder is indeed random for all concentrations in this salt.

The question of substitutional *vs.* positional disorder was elegantly addressed in the β″-$(BEDT\text{-}TTF)_2(SF_5\text{-}R\text{-}SO_3)$ series known to exhibit superconducting (R = CH_2CF_2), metallic (R = CHF), or metal–insulator (R = $CHFCF_2$) character.[88] With the latter chiral $SF_5CHFCF_2SO_3^-$ anion, positional disorder of the two enantiomers is observed in the pure phase and two characteristic, low-energy electronic excitations (centered at ≈5200 and 9600 cm^{-1}) were tentatively attributed to either correlation-driven or disorder-related localization. To test this assumption, solid solutions were prepared. When combining the superconducting (R = CH_2CF_2) and metallic (R = CHF) systems, only positional disorder is expected. The strongest charge-transfer excitations are observed for x = 0.5 where positional disorder is indeed maximum. On the other hand, when combining the superconducting (R = CH_2CF_2) with the metal–insulator (R = $CHFCF_2$) chiral anion, it appears that local orientational disorder effects (chiral anion) are much stronger than positional effects (alloying) as the strongest charge-transfer excitations are observed for x = 1. This demonstrates that the anion pocket disorder results in large-amplitude modulations of the electrostatic potential, which are very effective in localizing charge on the BEDT-TTF stack, revealed by these low-energy electronic excitations.

A specific situation needs to be mentioned where order emerges from disorder for the 50 : 50 composition, for example in $[(TMTSF)_{1-x}(TMTTF)_x]_2ReO_4$ for $x \approx 0.50$.[41] Independently of the $q_1 = (\frac{1}{2}, \frac{1}{2}, \frac{1}{2})$ superstructure associated with well-known anion ordering (AO) transition observed at low temperatures in both pure compounds and the alloys, another $q_2 = (0, \frac{1}{2}, \frac{1}{2})$

superstructure found already at room temperature has been attributed to an alternate order of the TMTTF and TMTSF molecules along the stacks, with a spatial coherence of $\approx$300 Å.

2.5 Tools for analyzing solid solutions' compositions

The evaluation of the exact composition and nature of solid solutions is a complex challenge. Several points are indeed of interest for any analytical method aimed at determining the alloy composition, such as its precision (important for low x values), its spatial extension, its reproducibility also in relation to the homogeneity of the samples themselves, and its eventual destructive character.

Energy-dispersive X-ray spectroscopy (EDS, EDX, EDXS or XEDS), sometimes called energy dispersive X-ray analysis (EDXA or EDAX) or energy dispersive X-ray microanalysis (EDXMA), has been the analytical technique of choice to analyze most solid solutions. Different elements can be probed simultaneously: for example, S *vs.* Se in $(TSF)_x(TTF)_{1-x}(TCNQ)$,[34] $[(TMTSF)_{1-x}(TMTTF)_x]_2PF_6$,[43] and κ-$[(ET)_{1-x}(BEDSeT\text{-}TTF)_x]_2Cu[N(CN)_2]Br$.[45]

X-Ray diffraction on single crystals is a useful tool when the two mixed species differ notably by their electron count and hence their diffracting power. Typical examples involve refinement of Cl^- *vs.* Br^- in $(o\text{-}Me_2TTF)_2Cl_{1-x}Br_x$,[68] Br *vs.* CH_3 in $[(Me_2)_{1-x}(MeBr)_x\text{-}DCNQI]_2Cu$,[60] Ni *vs.* Pd in $[(CH_3)_4N][Ni_xPd_{1-x}(dmit)_2]_2$,[57] and Pt *vs.* Au in $(Perylene)_2[Au_{1-x}Pt_x(mnt)_2]$.[49] The method, however, requires that a complete data set is collected and refined for each composition, while EDS methods (see above) provide comparable precision in a much faster way. On the other hand, the method gives a precise indication of the evolution of the structure (unit cell, molecular orientations) with x.

Inductively coupled plasma atomic emission spectroscopy (ICP-AES) has been used only rarely and is mentioned to evaluate the beryllium amount in the $[PLY\text{-}(O,O)]_2B_{1-x}Be_x$ solid solutions of spiro-bis(9-oxidophenalenone)boron $[PLY(O,O)]_2B$ with the neutral beryllium analog $[PLY(O,O)]_2Be$.[53,54]

Neutron activation analysis (NAA) has been reported by two groups to analyze solid solutions, in mixed crystals of (BEDT-TTF)-trihalides such as β-$(ET)_2(I_3)_{1-x}(IBr_2)_x$, β-$(ET)_2(IBr_2)_{1-x}(I_2Br)_x$ and β-$(ET)_2(I_2Br)_{1-x}(I_3)_x$ to determine the atomic ratio of bromine to iodine,[77,78] and in the extensive series of $(DCNQI)_2Cu$ salts to analyze Br and Cu.[61]

Elemental analysis can be used but its precision is relatively low; it requires large amounts of materials, most often not available when obtained by electrocrystallization. The method has therefore been limited to materials obtained in larger quantities by chemical routes, as in the series of $(DCNQI)_2Cu$ salts,[61] or in magnetic salts such as $[NO_2BzPy][Au_xNi_{1-x}(mnt)_2]$, where $[NO_2BzPy]^+$ stands for 1-(4′-nitrobenzyl)pyridinium and $[M(mnt)_2]^-$ for bis(maleonitriledithiolato)metallate.[55,56]

Mass spectrometry (EI-MS) has been used to discriminate between closely related molecular species, as between EDO-TTF and MeEDO-TTF in $[(EDO\text{-}TTF)_{1-x}(MeEDO\text{-}TTF)_x]_2PF_6$ where the two molecules only differ by a methyl group.[46] Experimental deviations of the x value were $\approx$0.01–0.02. It should be noted that the estimation of x values by this method bear some systematic error since the efficiencies of EDO-TTF and MeEDO-TTF molecules to produce molecular ions are different from each other. The same method was used for the mixed-valence $[Pd(dmit)_2]$ salts with mixtures of Me_4Sb^+, $EtMe_3Sb^+$ and $Et_2Me_2Sb^+$ cations.[67]

Solution NMR has been reported in one recent example for $(TMTSF)_2(TaF_6)_{1-x}(PF_6)_x$ solid solutions involving TaF_6^- and AsF_6^- anions thanks to ^{19}F NMR measurements of solutions prepared by dissolving small amounts of all materials in DMSO-d_6.[76] The integration of the signal of PF_6^-, appearing as a doublet at −70 ppm with respect to the signals of fluorine atoms connected to Ta(v), provided the TaF_6^-/PF_6^- ratio in the bulk material. Satisfyingly, the ratios estimated by this method were in good agreement with those obtained by the refinement of the single crystal diffraction data.

3. Manipulation of physical properties in solid solutions

Investigations of solid solutions in molecular conductors are associated with a variety of objectives, which concern the analogy with external pressure (chemical pressure) effects, the influence of disorder and/or doping on conductivity and eventually superconductivity, the manipulation of band filling, the insertion of magnetic defects, and the evolution of structural and/or electronic phase transitions characteristic of the pure compounds. These effects proved to be very complex to analyze and they will be illustrated in the following by only some representative examples.

3.1 Chemical pressure effects

Once the actual composition of the solid solution (x value in crystal) has been determined (*cf.* Section 2.5), it is possible to follow the evolution of the unit cell parameters with x. In the only situations where both pure compounds have the same crystal structure, a linear evolution of these parameters between the $x = 0$ and $x = 1$ situations is often observed, referred to as Vegard's law. Typical examples are reported, for example, in $(TMTSF)_2(ClO_4)_{1-x}(ReO_4)_x$,[71] θ-$(BEDT\text{-}TTF)_2(Rb_{1-x}Cs_x)Zn(SCN)_4$,[86] $(o\text{-}DMTTF)_2Br_xCl_{1-x}$,[68] and β-$(BEDT\text{-}TTF)_2(I_3)_{1-x}(IBr_2)_x$.[77,78] These linear evolutions are often described, in a misuse of language, as chemical pressure effects, as in most cases the actual evolutions of the pure systems under pressure are not known. In other words, the compressibility (and its anisotropy) of a pure system might be notably different from its evolution in a solid solution upon insertion of a smaller species. An illustration is provided by the β-$(ET)_2(I_3)_{1-x}(IBr_2)_x$ alloy where the smooth evolution of the unit cell parameters (contraction with increasing amount of the smaller IBr_2^- anion) parallels that observed in the pure β-$(ET)_2I_3$ phase ($x = 0$) under pressure between 0 and 4 kbar. The pure IBr_2^- phase ($x = 1$) is indeed crystallographically comparable to the $x = 0$ I_3^- phase at 4 kbar.[77] The situation is more delicate in the κ-$(BEDT\text{-}TTF)_2Cu[N(CN)_2]Br_xCl_{1-x}$ system,[83,85] where increasing amounts of Br^- anions do have the same effect as that of the physical pressure on the pure chloride salts ($x = 0$), while the unit cell volume is actually increasing (negative chemical pressure) with x.

Deviations from Vegard's law are common and can be indicative of the evolution of the molecular orientations such as the tilt angle of the stacks in $(TSeF)_x(TTF)_{1-x}$·TCNQ.[34] Such displacements are characteristic of molecular alloys and can have important consequences on the physical properties up to the point where a continuous change in composition can have non-linear effects on the structural and hence electronic properties. This is beautifully illustrated in the behavior of solid solutions of the $(DCNQI)_2Cu$ salts. Indeed, two groups emerge from this family: those with a stable metallic state down to low temperatures as found with Me_2DCNQI and I_2DCNQI, and those with a sharp metal–insulator transition as found with $Me_2DCNDI\text{-}d_8$, MeBrDCNQI and MeClDCNQI.[58–61] The first group is sensitive to pressure and undergoes a metal–insulator transition at a very low pressure ($\approx$50 bar) in $(Me_2DCNQI)_2Cu$ but a notably higher one (15.3 kbar) in the I_2DCNQI salt, indicating a very stable metallic state in the latter. Solid solutions combining two acceptors from group I, or two acceptors from group II, led to the expected group I or group II behavior respectively.[61,62] On the other hand, combining two acceptor molecules, one from each group, into solid solutions was reported for example in $[(Me_2)_{1-x}(MeBr)_xDCNQI]_2Cu$, where a small doping range ($x < 0.1$) was already sufficient to favor the occurrence of the M–I transition, with re-appearance of the metallic phase at lower temperatures. This behavior was already known for the pristine $(Me_2DCNQI)_2Cu$ under pressure.[59] The main origin of these evolutions is, however, to be found in the evolution of the structure itself, with the α angle characterizing the tetrahedral coordination around the Cu ion which exhibits a notable increase with MeBrDCNQI concentration (Fig. 3).[59] This sensitivity varies with the nature of the acceptors. In the $[(MeIDCNQI)_{1-x}(MeBrDCNQI)_x]_2Cu$ alloy, the group I behavior of $(MeIDCNQI)_2Cu$ was for example maintained up to $x = 0.60$.[61] These examples illustrate how prudent one should be when referring to chemical pressure effects.

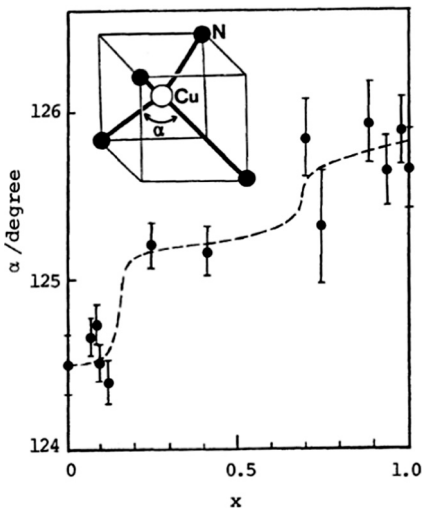

Fig. 3 Evolution of the α angle with x in the coordination sphere of Cu in the $[(Me_2)_{1-x}(MeBr)_xDCNQI]_2Cu$ alloys. Taken from ref. 59. © 1989 The Chemical Society of Japan.

Another convincing illustration is provided by $[(Me_2DCNQI)_{1-x}\text{-}(Me_2DCNQI\text{-}d_8)_x]_2Cu$ alloys involving the deuterated $Me_2DCNQI\text{-}d_8$ belonging to group II. This system clearly reproduced the low-pressure region (1–500 bar) of the exotic pressure–temperature phase diagram of $[Me_2DCNQI]_2Cu$ including the reentrant M–I–M transition at ambient pressure.[58] The sharp transitions observed in the resistivity measurements indicated that the system is homogeneous and that the disorder effect brought by deuteration was reduced here to a minimum, which cannot be realized in other alloyed $(DCNQI)_2Cu$ salts. In this case, the very high sensitivity of the $[Me_2DCNQI]_2Cu$ system to pressure and the chemical pressure control using the deuteration were the key elements for reproducing with alloying the pressure–temperature diagram of the pure hydrogenated system.

3.2 Anion ordering transitions

Since TMTTF/TMTSF (Fabre/Bechgaard) salts crystallize in the $P\bar{1}$ space group with the counter ion located at the inversion center, non-centrosymmetric anions such as ReO_4^- and ClO_4^- are disordered at room temperature. At low temperatures, they order in such a way that neighboring anions align or alternate their orientation. In $(TMTSF)_2ReO_4$, the anions alternate in the three crystallographic directions below $T_{AO} = 176$ K, an ordering characterized by a reduced wave vector $q_1 = (\frac{1}{2}, \frac{1}{2}, \frac{1}{2})$. In $(TMTSF)_2ClO_4$, the AO is found at $q_2 = (0, \frac{1}{2}, 0)$ with a much lower T_{AO} value (24 K), indicating an average decrease of the electron–anion coupling, with the ClO_4^- anions having weaker interactions with the TMTSF stacks than the ReO_4^- ones.[70] In $(TMTSF)_2(ReO_4)_{1-x}(ClO_4)_x$ solid solutions,[71] it was shown that the q_1 long range order (LRO) of the ReO_4^- phase ($x = 0$) was maintained for $x < 0.5$, while the q_2 LRO of the ClO_4^- phase ($x = 1$) was destroyed for $x < 0.97$. For the intermediate $0.5 < x < 0.97$ compositions, the complex coexistence of short range orders (SRO) at q_1 and q_2 is observed. The phase diagram of this solid solution was analyzed within the framework of an Ising model, with an Ising variable $\eta_i = \pm 1$ depending on the anion orientation.

3.3 Alloying effects on conductivity

The conductivity of solid solutions is almost systematically investigated but its evolution with alloy composition and with temperature can be extremely complex to analyze as it depends on many different factors. We need for example to distinguish here two situations, those related to weak doping with x values close to 0 or 1, and those related to systems where x continuously covers the whole spectrum between 0 and 1. We will concentrate here on the second situation, and illustrate it first with the prototypical TTF·TCNQ system and its solid solution with TSF. As shown in Fig. 4, the RT conductivity is decreased in the solid solution by comparison with the pure salts, a consequence of disordering the donor stack. This effect of disorder due to alloy formation also manifests itself in a smaller increase in conductivity with decreasing temperature. The conductivity increases indeed for the solid solutions by 7–10 times in going from room temperature to the temperature T_{MI} at which it peaks (Peierls transition), compared to values for TTF·TCNQ and TSF·

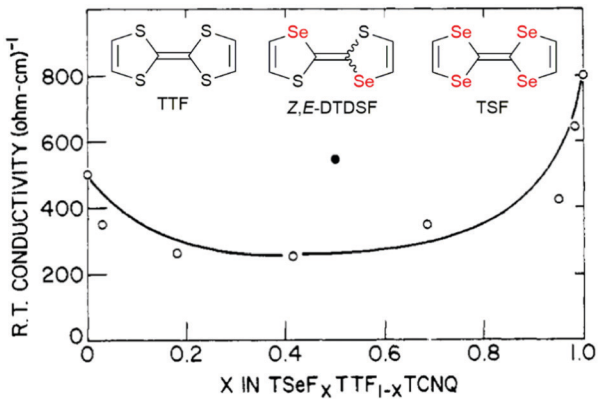

Fig. 4 Room temperature conductivity of $(TSF)_x(TTF)_{1-x}(TCNQ)$ (open circles). The closed black circle refers to [(*Z*,*E*)-DTDSF]TCNQ (see text). Adapted from ref. 34. © 1977 American Chemical Society.

TCNQ (12–20 times). Furthermore, the dominance of the TCNQ stacks and the unimportance of fulvalene disorder in producing the metal–insulator transition are confirmed for $0 < x < 0.9$,[36] as only 3% incorporation of TSF into TTF–TCNQ completely obscures the 38 K transition associated with the TTF fstacks in TTF–TCNQ, while the 53 K transition remains relatively sharp.[34] These evolutions are compared with those observed in an analogous salt isolated with the (*Z*,*E*-DTDSF)·TCNQ (see Fig. 4). The notably higher RT conductivity of (*Z*,*E*-DTDSF)·TCNQ than that of the 50 : 50 solid solution indicates that the donor stack conductivity is much less affected by disorder due to the random arrangement of *Z*- and *E*-DTDSF molecules than that of the TSF and TTF molecules. This is because both *Z*- and *E*-DTDSF molecules are electronically very close, at variance with TSF and TTF whose oxidation potential differs by 0.17 V.[36]

Another example of the effect of disorder on the phase diagram is provided by $(TMTTF)_2(SbF_6)_{1-x}(AsF_6)_x$ solid solutions. At low temperatures, a non-magnetic (spin-Peierls) ground state is reported for $(TMTTF)_2AsF_6$, while an antiferromagnetic ground state characterizes the pure SbF_6^- salt. The $(TMTTF)_2(SbF_6)_{1-x}(AsF_6)_x$ alloys behave as pure salts for $x < 0.2$ and $x > 0.8$, while in the middle range, higher disorder prevents the condensation of any ordered phase.[74]

3.4 Alloying effects on superconductivity

The well-known sensitivity of superconductivity to disorder or defects was investigated soon after it was discovered at ambient pressure in $(TMTSF)_2ClO_4$. It was indeed shown that introduction of only 5% TMTTF in $[(TMTSF)_{1-x}(TMTTF)_x]_2ClO_4$ was sufficient to suppress the superconductivity.[40] On the other hand, when replacing the ClO_4^- anion with a nominal concentration of ReO_4^- up to x = 0.06 in $(TMTSF)_2(ClO_4)_{1-x}(ReO_4)_x$, the superconducting transition temperature is decreased by a factor of about two.[72a,b]

β-$(BEDT\text{-}TTF)_2I_3$ is the first superconductor in the I_3^- salts of BEDT-TTF and was intensively studied at an early stage.[23] The coexistence of high-T_c and low-T_c states was a puzzle that is related to an incommensurate lattice modulation below 200 K. In order to clarify this problem, an alloy system with the superconducting β-$(BEDT\text{-}TTF)_2AuI_2$ salt, β-$(ET)_2(I_3)_{1-x}(AuI_2)_x$ (x = 0.1, 0.9), was examined by low-temperature X-ray diffraction and transport measurements.[79,81] It was suggested that two types of disorder, namely the conformational disorder of the terminal ethylene groups and the distortions in the anion sites, can affect the superconducting state. The superconductivity was destroyed in the x = 0.1 and x = 0.6 alloys, while in the AuI_2^- rich phase (x = 0.9), stepwise resistivity drops were observed at 4.5 and 2.1 K. The high-temperature anomaly at 4.5 K has been attributed to the high-T_c anomaly of β-$(BEDT\text{-}TTF)_2I_3$ and the superconducting transition at 2.1 K will correspond to the low-T_c transition.

In β-$(BEDT\text{-}TTF)_2(I_3)_{1-x}(IBr_2)_x$ alloys, the superconductivity of the pure I_3^- phase was destroyed already for x = 0.05 and above, while on the other side of the alloy, the superconducting state of the pure IBr_2^- phase was maintained for $x \geq 0.75$.[77] In that respect, the superconductivity of the so-called κ-Br phase of BEDT-TTF, *i.e.* κ-$(BEDT\text{-}TTF)_2Cu[N(CN)_2]Br$, appears to be particularly robust as substitution of the donor molecule with the diselenated BEDT-SFT analog (see Scheme 2) allowed maintaining the superconductivity for x values up to 0.20 in κ-$[(BEDT\text{-}TTF)_{1-x}(BEDT\text{-}STF)_x]_2Cu[N(CN)_2]Br$.[44]

Similar disorder/size effects on superconductivity have been reported in the superconducting K_3C_{60}. The superconducting temperature of the pure compound K_3C_{60} at 19 K was progressively reduced upon alloying it with C_{70} in $K_3(C_{60})_{1-x}(C_{70})_x$ and the SC state disappeared for $x > 0.25$.[63]

3.5 Band filling manipulation

At variance with inorganic (super)conductors where band filling can be easily modified, for example through oxygen doping in high-T_c superconductors, molecular conductors with their fixed stoichiometry are most often not amenable to such strategies. Attempts have been reported, however, (i) in cation-radical salts upon replacement of a monovalent anion with a divalent one ($GaCl_4^-/FeCl_4^-$ *vs.* $MnCl_4^{2-}/CoCl_4^{2-}$),[87,98,111] (ii) in anion radical salts upon replacement of Cu^+/Cu^{2+} with Li^+ and (iii) in single component conductors where neutral metallic complexes are mixed with analogous neutral complexes having different electron counts.

Modification of band filling in cation radical salts proved to be very difficult as most often the structure resists the insertion of a divalent anion in place of a monovalent one. This strategy was successfully investigated, for example, in BEDT-TTF salts such as λ-$(ET)_2(GaCl_4)_{1-x}(CoCl_4)_x$ with $x < 0.06$ and in δ′-$(ET)_2(GaCl_4)_{1-x}(CoCl_4)_x$ with $x < 0.14$. In both systems, at maximum doping, the RT conductivity was found to decrease by one order of magnitude relative to the pure $GaCl_4^-$ salts.[87] The most successful examples were reported from TTM-TTP salts, which are known to crystallize not only with monovalent anions ($FeCl_4^-$, $GaCl_4^-$) to give 1 : 1 phases, *i.e.* with a ρ = 1 charge transfer and associated $\frac{1}{2}$ band filling and a metallic character at RT, but also with divalent anions ($MnCl_4^{2-}$, $CoCl_4^{2-}$) with the same 1 : 1 stoichiometry and regular stacking but now with ρ = 2, zero band-filling and semiconducting character.[98] Three alloys prepared by combining $CoCl_4^{2-}$ with either $FeCl_4^-$ or $GaCl_4^-$ in $(TTM\text{-}TTP)Fe_{1-x}Co_xCl_4$ (x = 0.05, 0.40)

and (TTM-TTP)$Ga_{1-x}Co_xCl_4$ (x = 0.30) were reported. The decreased band filling associated with increasing x values was correlated with a regular increase of the room-temperature resistivity and thermoelectric power.

In radical anion salts, the $Cu(DCNQI)_2$ system is also a beautiful example of variable doping in the solid solutions where the copper is substituted with Li^+. Indeed, in the pure $Cu(DCNQI)_2$ salt, the valence of the copper is intermediate (+1.3) between those of Cu^+ and Cu^{2+}. Replacing progressively copper with Li^+ hence modifies continuously the band filling and turns the metallic $Cu(DCNQI)_2$ system into a semiconductor in the whole temperature range (Fig. 5).[65,66]

Single-component conductors offer another possibility for modifying the band filling, as illustrated below in several examples where neutral complexes with different electron counts can be mixed. For example, $[Ni(tmdt)_2]$ (see Scheme 1) is a 3D metal stable down to 4 K, while $[Au(tmdt)_2]$, bearing one extra electron, is reported to undergo an antiferromagnetic transition around 110 K ($T_{Néel}$) without loss of its high conductivity. The temperature dependence of the resistivities of the compressed pellet samples of $[Ni_{1-x}Au_x(tmdt)_2]$ alloys[51] ($0 < x < 1$) showed the systems to be essentially metallic down to low temperature, while $T_{Néel}$ was moved to lower temperatures with decreasing x value, essentially disappearing for $x \leq 0.6$. Moving to solid solutions involving the isoelectronic copper analog $[Cu(tmdt)_2]$ rather than the gold one gives a fully different picture,[52] as the extra electron in $[Cu(tmdt)_2]$ is now localized in an antibonding metal–ligand orbital with $d_{x^2-y^2}$ symmetry. The magnetic behavior of $[Ni_{1-x}Cu_x(tmdt)_2]$ for x = 0.098, 0.13 and 0.18 was described as a molecular Kondo system, while, at a higher copper concentration (x = 0.27), the magnetic moments begin to interact antiferromagnetically with each other through the so-called π–d interaction.

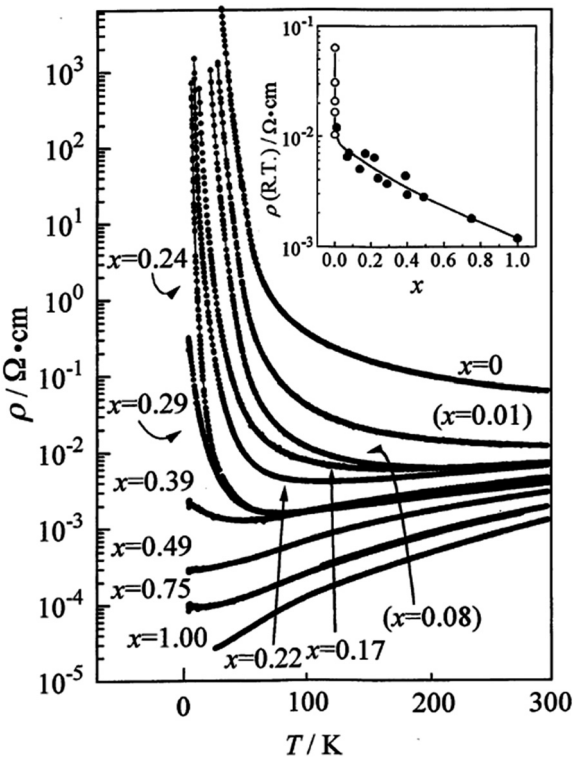

Fig. 5 Temperature dependence of the resistivity of $(DMDCNQI)_2Li_{1-x}Cu_x$. The inset shows the dependence of resistivity at RT with the white circles for the x = 0 compound with various impurity levels. Reproduced from ref. 66. © 1999 The Physical Society of Japan.

The situation is also rather complex in phenalenyl-based single-component conductors such as $[PLY(O,O)]_2B$ (see Scheme 1).[53,54] The radical complex can be substituted with the diamagnetic beryllium analog lacking this extra electron. At low doping levels ($x \leq 0.15$), substitutional doping is effective and increases the conductivity while lowering the activation energy of both compounds. Higher doping proved to be more difficult as the beryllium analog is not isostructural with its boron congeners, a striking consequence of this different electron count. It has been argued that this effect on the conductivity cannot be described as a classical semiconductor hole doping as the energy levels of the beryllium dopant are not located in the semiconducting gap of the boron complex. The increase in conductivity would rather be a consequence of decreased antiferromagnetic interactions between pairs of boron radicals.

3.6 Alloying effects on magnetic properties

Because of the strong electronic correlations present in these conducting systems (especially in Mott insulators), specific magnetic properties are closely related to these conducting properties and their evolution within solid solutions provides another extremely rich tool for exploring phase diagrams. One first example is provided by the TMTTF salts with either AsF_6^- or SbF_6^-.[74,75] While the AsF_6^- salt exhibits a non-magnetic (spin-Peierls) ground state below 14 K, the SbF_6^- salt gives rise to an antiferromagnetic ground state below $T_{Néel}$ = 8 K. At higher temperatures, the resistivity of $(TMTTF)_2SbF_6$ shows clear evidence of an anomaly around T_ρ = 154 K, below which $d\rho/dT$ becomes negative, where ρ is the resistivity. This semiconducting charge-ordered phase (below T_ρ) gradually weakens by alloying it with AsF_6^-,[74b] but proved to be present in all compositions.[75] First experiments on $(TMTTF)_2[(AsF_6)_x(SbF_6)_{1-x}]$ solid solutions using electron spin resonance (ESR) and magnetic susceptibility have detected the antiferromagnetic phase transition and the spin-gap transition near the pure AsF_6^- and SbF_6^- salts, respectively, that is for $x > 0.8$ and $x < 0.2$, while the absence of any ordered ground state was postulated in the intermediate ($x \approx 0.5$) region.[74c] ^{13}C NMR studies of the ground states and critical behavior in this alloy system for x = 0.3, 0.5 and 0.67 suggested, however, that the antiferromagnetic phase and spin-gap phase are in contact at low temperatures. The x = 0.5 alloy is situated on the edge of the spin-gap phase, showing a gradual phase transition and significant critical fluctuations at low temperatures, which can be attributed to the quantum critical effect.

Another example is the alloyed quantum spin liquid system based on salts of $Pd(dmit)_2$.[112] Indeed, the anion radical salt $EtMe_3Sb[Pd(dmit)_2]_2$ is a Mott insulator with a triangular lattice where the spin frustration plays an important role. By changing the cation, the degree of frustration can be tuned without

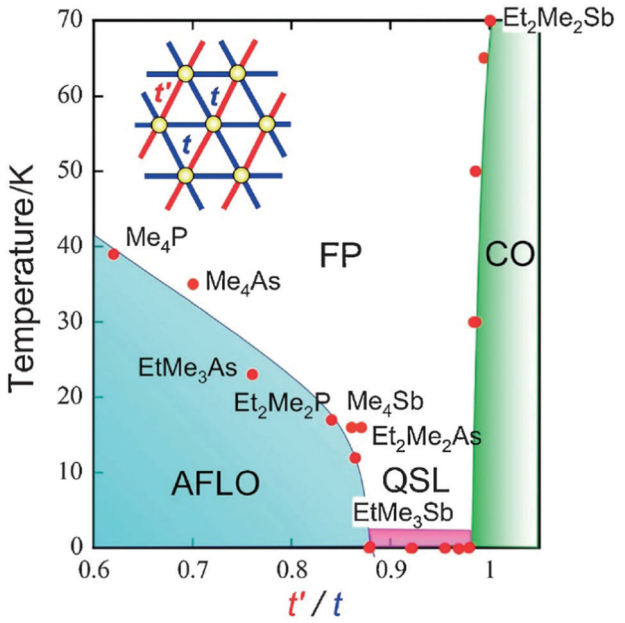

Fig. 6 Phase diagram for the series of β′-X[Pd(dmit)$_2$]$_2$ salts. Points referring to the $(Me_4Sb)_{1-x}(EtMe_3Sb)_x[Pd(dmit)_2]_2$ and $(Et_2Me_2Sb)_{1-x}(EtMe_3Sb)_x[Pd(dmit)_2]_2$ solid solutions are those located between t'/t = 0.87 (for pure Me_4Sb^+ salt) and t'/t = 1 (for pure $Et_2Me_2Sb^+$ salt), with the pure $EtMe_3Sb^+$ salt at t'/t = 0.92. Abbreviations: FP, frustrated paramagnetic (state); AFLO, antiferromagnetically long-range ordered (state); CO, charge-ordered (state); QSL, quantum spin liquid (state). Reproduced from ref. 112. © 2014 The Chemical Society of Japan.

serious changes in the crystal structure. The magnetic ground state of this Mott system depends on the degree of frustration, characterized by the t'/t ratio of interdimer transfer integrals t and t' (see Fig. 6). With the smaller Me_4Sb^+ cation, the salt shows an antiferromagnetic long-range order (AFLO), while with the larger $Et_2Me_2Sb^+$ cation, the salt exhibits a non-magnetic charge-order state (CO). The alloying of the $EtMe_3Sb^+$ salt with either Me_4Sb^+ or $Et_2Me_2Sb^+$ cations changes lattice constants[67] and the degree of frustration continuously. This alloyed system conformed to a phase diagram where the quantum spin liquid exists as a ''phase'' (not a critical ''point'') located between the antiferromagnetic phase and the charge order phase as shown in Fig. 6.

3.7 Magnetic doping

Another sought-after strategy for the preparation of solid solutions of molecular conductors is the sequential introduction of localized magnetic ions in the neighborhood of a conducting stack. Perhaps one of the first experimental demonstrations was reported in the perylene salts $(Per)_2[Pt_xAu_{1-x}(mnt)_2]$, where the anionic chains of $[M(mnt)_2]^-$ complexes are either diamagnetic (M = Au) or paramagnetic (M = Pt).[47,48] Both pure compounds, in their α-phase, present a metal-to-insulator transition at 8 K and 12 K, respectively, which has been ascribed to the Peierls distortion (tetramerisation) of the perylene chains. The Pt compound presents, in addition to the Peierls transition involving the conducting perylene chains, a spin-Peierls transition at the same critical temperature that corresponds to the dimerization of the spin-carrying units $[Pt(mnt)_2]^-$.[113] This metallic α-phase was still observed in the alloys for $x < 0.50$ and $x > 0.95$, while in the intermediate range $0.50 \leq x \leq 0.95$, the salt adopts another structural β-type associated with a semiconducting behavior in the whole temperature range.[49]

One of the most investigated systems along these lines is λ-$(BETS)_2MCl_4$ where the diamagnetic $GaCl_4^-$ anion can be substituted with the high-spin Fe^{III} $FeCl_4^-$ anion (S = 5/2).[92,93] Indeed, λ-$(BETS)_2GaCl_4$ undergoes a superconducting transition at ≈6 K, and the superconductivity is destroyed under a magnetic field of 13 T parallel to the conduction plane. On the other hand, its isostructural analogue λ-$(BETS)_2FeCl_4$ exhibits a coupled metal–insulator and antiferromagnetic transition at 8.5 K, suggesting the important role of the interaction between the π electrons of BETS and the d electrons of the high-spin Fe^{3+} ion. The insulating phase for λ-$(BETS)_2FeCl_4$ is destabilized by the magnetic field above ≈10 T, where the paramagnetic state of the Fe moments is recovered. A complete phase diagram is shown in Fig. 7.

The field-induced superconductivity for λ-$(BETS)_2FeCl_4$ has been understood in terms of the Jaccarino–Peter effect,[114] in which the internal magnetic field due to the exchange interaction with localized Fe moments is crucial. In $(BETS)_2Fe_xGa_{1-x}Cl_4$ alloys,[94] superconductivity is observed only under very high magnetic fields parallel to the conducting layer for $x \geq 0.47$ (Fig. 8). As x decreases, the field induced superconducting phase shifts towards lower fields and a striking field-induced insulator to superconductor transition is observed below 4 T for x = 0.45.

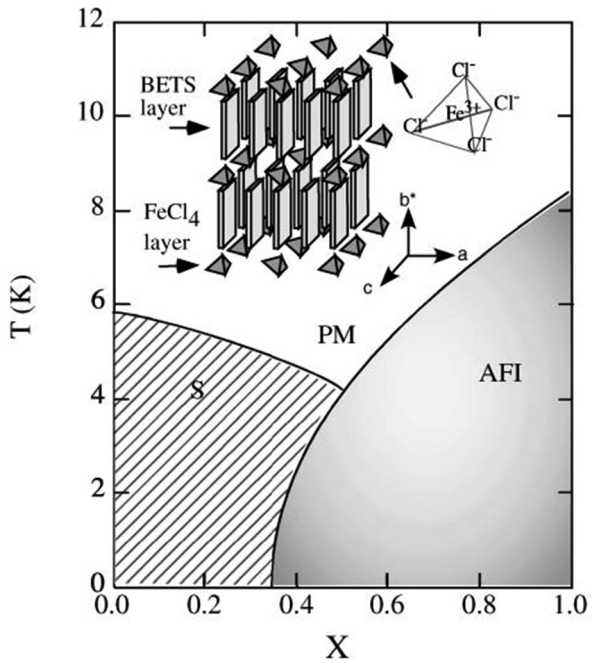

Fig. 7 Phase diagram of the organic alloys λ-$(BETS)_2Fe_xGa_{1-x}Cl_4$ in the absence of an external magnetic field. PM, AFI and S denote paramagnetic metal, antiferromagnetic insulator and superconductor, respectively. Reproduced from ref. 94. © 2003 The Physical Society of Japan.

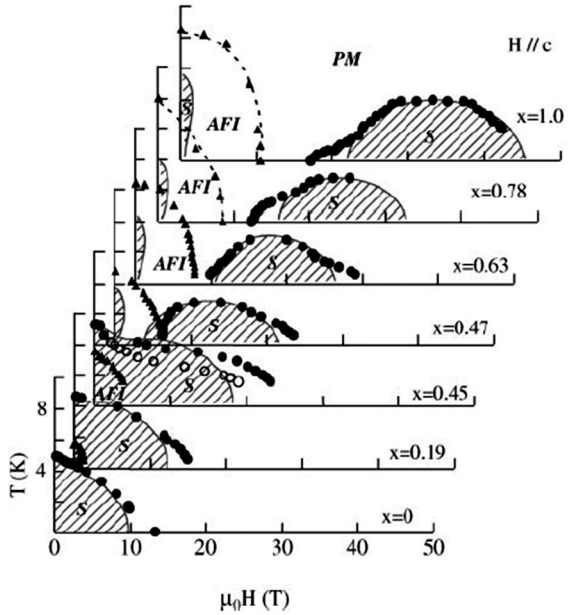

Fig. 8 Global magnetic phase diagram of λ-$(BETS)_2Fe_xGa_{1-x}Cl_4$ under fields applied parallel to the *c* axis. The PM–S transition fields are defined as the midpoints of the resistive transitions (closed circles), and the AFI–PM or AFI–S transition fields are given by the onset of a sharp change in resistance (triangles). For $x = 0.45$, the onset of the steep change in the PM–S transition is also plotted with open circles for comparison. The phase boundaries shown by circles and triangles are second and first order transitions, respectively. The shaded areas show the superconducting phases. Reproduced from ref. 94. © [2003] The Physical Society of Japan.

4. Conclusions

Solid solution strategies in molecular conductors have been considered since the very beginning of this active research area as an invaluable tool for modulating, in a continuous way, the structural and electronic properties of these materials. Such crystalline molecular conductors are characterized by specific properties such as (i) fixed stoichiometry, (ii) low dimensionality, (iii) limited band dispersions, (iv) strong electron correlations and (v) high compressibility. As a consequence, their electronic structure is generally highly sensitive to not only minute modifications of the solid-state organization, with strong effects of external pressure, but also composition modifications such as those brought by solid solutions. Both cation and anion radical salts, and single-component conductors, have been modified upon alloying and often in the whole composition range, even if novel crystal growth conditions are sometimes needed.

Topics such as preferential insertion and miscibility, the nature of disorder and the different analytical tools used for characterizing these alloys have been presented, showing the often-overlooked complexity of these systems. The consequences of alloying on conductivity and on phase transitions (superconductivity, anion ordering, Peierls transition, spin-Peierls transition, antiferromagnetic ground state), and the concepts of chemical pressure effects, band filling manipulation, and π–d interactions with magnetic anions have been discussed. In many instances, however, it proved to be difficult to sort out which peculiarity of the solid solutions is at the origin of the physical properties' evolution. This complexity makes use of solid solutions a difficult but extremely rich strategy to also investigate the electronic properties of pure compounds, even if we feel that the structural properties of solid solutions themselves require in most cases deeper investigations.

Conflicts of interest

There are no conflicts to declare.

Acknowledgements

We thank past and current colleagues for discussions on this topic, P. Batail (Orsay, Nantes, Angers), C. Lenoir (Orsay), K. Boubekeur (Orsay, Nantes), R. Clérac (Bordeaux), C. Mézière (Nantes, Angers), O. Jeannin (Rennes) and S. Bertaina (Marseille). Financial support was granted by ANR (France) under contract number ANR-20-CE29-0011-02.

Notes and references

1 M. Lusi, *Cryst. Growth Des.*, 2018, **18**, 3704–3712.
2 S. Aitipamula, R. Banerjee, A. K. Bansal, K. Biradha, M. L. Cheney, A. Roy Choudhury, G. R. Desiraju, A. G. Dikundwar, R. Dubey, N. Duggirala, P. P. Ghogale, S. Ghosh, P. Kumar Goswami, N. Rajesh Goud, R. R. K. R. Jetti, P. Karpinski, P. Kaushik, D. Kumar, V. Kumar, B. Moulton, A. Mukherjee, G. Mukherjee, A. S. Myerson, V. Puri, A. Ramanan, T. Rajamannar, C. Malla Reddy, N. Rodriguez-Hornedo, R. D. Rogers, T. N. Malla Row, P. Sanphui, N. Shan, G. Shete, A. Singh, C. C. Sun, J. A. Swift, R. Thaimattam, T. S. Thakur, R. Kumar Thaper, S. P. Thomas, S. Tothadi, V. R. Vangala, N. Variankaval, P. Vishweshwar, D. R. Weyna and M. J. Zaworotko, *Cryst. Growth Des.*, 2012, **12**, 2147–2152.
3 X. Huang, X. Liu, K. Ding and S. R. Forrest, *Mater. Horiz.*, 2020, **7**, 244–251.
4 C. R. Adolf, S. Ferlay and M. W. Hosseini, *CrystEngComm*, 2018, **20**, 2233–2236.
5 K. T. Butler, A. Walsch, A. K. Cheetham and G. Kieslich, *Chem. Sci.*, 2016, **7**, 6316–6324.
6 X. Ding, D. K. Unruh, R. H. Groeneman and K. M. Hutchins, *Chem. Sci.*, 2020, **11**, 7701–7707.
7 F. Brivio, C. Caetano and A. Walsch, *J. Phys. Chem. Lett.*, 2016, **7**, 1083–1087.
8 M. Habgood, R. Grau-Crespo and S. L. Price, *Phys. Chem. Chem. Phys.*, 2011, **13**, 9590–9600.
9 J. Bouzaid, M. Schultz, Z. Lao, J. Bartley, T. Bostrom and J. McMurtrie, *Cryst. Growth Des.*, 2012, **12**, 3906–3916.
10 (*a*) M. Sorai, J. Ensling and P. Gütlich, *Chem. Phys.*, 1976, **18**, 199–209; (*b*) P. Gütlich, R. Link and H. G. Steinhauser, *Inorg. Chem.*, 1978, **17**, 2509–2514; (*c*) P. Gütlich, R. Link, H. Klippen and H.-G. Steinhauser, *J. Chem. Phys.*, 1979, **70**, 3977–3983; (*d*) O. Kahn and C. J. Martinez, *Science*, 1998, **279**, 44–48.

11 T. Tayagaki, A. Galet, G. Molnár, M. C. Muñoz, A. Zwick, K. Tanaka, J.-A. Real and A. Bousseksou, *J. Phys. Chem. B*, 2005, **109**, 14859–14867.
12 For recent examples, see: (*a*) F. J. Valverde-Munoz, M. Seredyuk, M. Meneses-Sanchez, M. C. Munoz, C. Bartual-Murguia and J. A. Real, *Chem. Sci.*, 2019, **10**, 3807–3816; (*b*) N. Paradis, F. Le Gac, P. Guionneau, A. Largeteau, D. S. Yufit, P. Rosa, J.-F. Létard and G. Chastanet, *Magnetochemistry*, 2016, **2**, 15; (*c*) M. S. Sylla, C. Baldé, N. Daro, C. Desplanches, M. Marchivie and G. Chastanet, *Eur. J. Inorg. Chem.*, 2018, 297–304; (*d*) C. Bartual-Murgui, C. Pérez-Padilla, S. J. Teat, O. Roubeau and G. Aromí, *Inorg. Chem.*, 2020, **59**, 12132–12142.
13 S. Chorazy, J. J. Stanek, W. Nogaś, A. M. Majcher, M. Rams, M. Kozieł, E. Juszyńska-Gałązka, K. Nakabayashi, S.-I. Ohkoshi, B. Sieklucka and R. Podgajny, *J. Am. Chem. Soc.*, 2016, **138**, 1635–1646.
14 J. Wang, Y. Suffren, C. Daiguebonne, S. Freslon, K. Bernot, G. Calvez, L. Le Pollès, C. Roiland and O. Guillou, *Inorg. Chem.*, 2019, **58**, 2659–2668.
15 L. M. Aguirre-Díaz, F. Gándara, M. Iglesias, N. Snejko, E. Gutiérrez-Puebla and M. A. Monge, *J. Am. Chem. Soc.*, 2015, **137**, 6132–6135.
16 G. Kieslich, S. Kumagai, A. C. Forse, S. Sun, S. Henke, M. Yamashita, C. P. Grey and T. Cheetham, *Chem. Sci.*, 2016, **7**, 5108–5116.
17 (*a*) H. Seo, C. Hotta and H. Fukuyama, *Chem. Rev.*, 2004, **104**, 5005–5036; (*b*) T. Giamarchi, *Chem. Rev.*, 2004, **104**, 5037–5055.
18 D. Jérôme, *Chem. Rev.*, 2004, **104**, 5565–5591.
19 H. Jiang, P. Hu, J. Ye, K. K. Zhang, Y. Long, W. Hu and C. Kloc, *J. Mater. Chem. C*, 2018, **6**, 1884–1902 and references therein.
20 (*a*) F. Wudl, G. Smith and E. Hufnagel, *J. Chem. Soc., Chem. Commun.*, 1970, 1453–1454; (*b*) J. Ferraris, D. O. Cowan, W. Walatka and J. Perlstein, *J. Am. Chem. Soc.*, 1973, **95**, 948–949.
21 T. Mori, *Chem. Rev.*, 2004, **104**, 4947–4969.
22 B. A. Scott, S. J. La Placa, J. B. Torrance, B. D. Silverman and B. Welber, *J. Am. Chem. Soc.*, 1977, **99**, 6631–6639.
23 R. P. Shibaeva and E. B. Yagubskii, *Chem. Rev.*, 2004, **104**, 5347–5378.
24 H. Kobayashi, H. B. Cui and A. Kobayashi, *Chem. Rev.*, 2004, **104**, 5265–5288.
25 C. Rovira, *Chem. Rev.*, 2004, **104**, 5289–5318.
26 (*a*) S. K. Pal, M. E. Itkis, F. S. Tham, R. W. Reed, R. T. Oakley and R. C. Haddon, *Science*, 2005, **309**, 281–284; (*b*) S. Mandal, S. Samanta, M. E. Itkis, D. W. Jensen, R. W. Reed, R. T. Oakley, F. S. Tham, B. Donnadieu and R. C. Haddon, *J. Am. Chem. Soc.*, 2006, **128**, 1982–1994.
27 (*a*) M. P. Andrews, A. W. Cordes, D. C. Douglass, R. M. Fleming, S. H. Glarum, R. C. Haddon, P. Marsh, R. T. Oakley, T. T. M. Palstra, L. F. Schneemeyer, G. W. Trucks, R. W. Tycko, J. V. Waszczak, K. M. Young and N. M. Zimmerm, *J. Am. Chem. Soc.*, 1991, **113**, 3559–3568; (*b*) A. W. Cordes, R. C. Haddon, R. G. Hicks, R. T. Oakley, T. T. M. Palstra, L. F. Schneemeyer and J. V. Waszczak, *J. Am. Chem. Soc.*, 1992, **114**, 1729–1732.
28 (*a*) A. A. Leitch, R. W. Reed, C. M. Robertson, J. F. Britten, X. Yu, R. A. Secco and R. T. Oakley, *J. Am. Chem. Soc.*, 2007, **129**, 7903–7914; (*b*) D. Tian, S. M. Winter, A. Mailman, J. W. L. Wong, W. Yong, H. Yamaguchi, Y. Jia, J. S. Tse, S. Desgreniers, R. A. Secco, S. R. Julian, C. Jin, M. Mito, Y. Ohishi and R. T. Oakley, *J. Am. Chem. Soc.*, 2015, **137**, 14136–14148.
29 (*a*) T. Isono, H. Kamo, A. Ueda, K. Takahashi, A. Nakao, R. Kumai, H. Nakao, K. Kobayashi, Y. Murakami and H. Mori, *Nat. Commun.*, 2013, **4**, 1344–1349; (*b*) A. Ueda, S. Yamada, T. Isono, H. Kamo, A. Nakao, R. Kumai, H. Nakao, Y. Murakami, K. Yamamoto, Y. Nishio and H. Mori, *J. Am. Chem. Soc.*, 2014, **136**, 12184–12192.
30 Y. Kobayashi, T. Terauchi, S. Sumi and Y. Matsushita, *Nat. Mater.*, 2017, **16**, 109–114.
31 (*a*) H. Tanaka, Y. Okano, H. Kobayashi, W. Suzuki and A. Kobayashi, *Science*, 2001, **291**, 285–287; (*b*) A. Kobayashi, E. Fujiwara and H. Kobayashi, *Chem. Rev.*, 2004, **104**, 5243–5264; (*c*) H. B. Cui, H. Kobayashi, S. Ishibashi, M. Sasa, F. Iwase, R. Kato and A. Kobayashi, *J. Am. Chem. Soc.*, 2014, **136**, 7619–7622.
32 (*a*) N. Tenn, N. Bellec, O. Jeannin, L. Piekara-Sady, P. Auban-Senzier, J. Iniguez, E. Canadell and D. Lorcy, *J. Am. Chem. Soc.*, 2009, **131**, 16961–16967; (*b*) Y. Le Gal, T. Roisnel, P. Auban-Senzier, N. Bellec, J. Iniguez, E. Canadell and D. Lorcy, *J. Am. Chem. Soc.*, 2018, **140**, 6998–7004.
33 (*a*) H. B. Cui, T. Tsumuraya, T. Miyazaki, Y. Okano and R. Kato, *Eur. J. Inorg. Chem.*, 2014, 3837–3840; (*b*) H. Hachem, H. B. Cui, T. Tsumuraya, R. Kato, O. Jeannin, M. Fourmigué and D. Lorcy, *J. Mater. Chem. C*, 2020, **8**, 11581–11592.
34 E. M. Engler, B. A. Scott, S. Etemad, T. Penney and V. V. Patel, *J. Am. Chem. Soc.*, 1977, **99**, 5909–5916.
35 (*a*) Y. Tomkiewicz, E. M. Engler and T. D. Shultz, *Phys. Rev. Lett.*, 1975, **35**, 456–459; (*b*) P. M. Chaikin, J. F. Kwak, R. L. Greene, S. Etemadt and E. M. Engler, *Solid State Commun.*, 1976, **19**, 1201–1204.
36 S. Etemad, E. M. Engler, T. D. Schultz, T. Penney and B. A. Scott, *Phys. Rev. B*, 1978, **17**, 513–528.
37 S. Ravy, J. P. Pouget and R. Comes, *J. Phys. I France*, 1992, **2**, l173–l190.
38 P. Alemany, E. Canadell and J.-P. Pouget, *Europhys. Lett.*, 2016, **113**, 27006.
39 (*a*) A. J. Epstein, J. S. Miller, J.-P. Pouget and R. Comès, *Phys. Rev. Lett.*, 1981, **47**, 741–744; (*b*) J.-P. Pouget, R. Comès, A. J. Epstein and J. S. Miller, *Mol. Cryst. Liq. Cryst.*, 1982, **85**, 203–213; (*c*) A. J. Epstein, J. W. Kaufer, H. Rommelmann, I. A. Howard, E. M. Conwell, J. S. Miller, J.-P. Pouget and R. Comès, *Phys. Rev. Lett.*, 1982, **49**, 1037–1041.
40 (*a*) C. Coulon, P. Delhaes, J. Amiell, J. P. Manteau, J. M. Fabre and I. Giral, *J. Phys.*, 1982, **43**, 1721–1729; (*b*) J. P. Pouget, R. Moret, R. Comes, G. Shirane, K. Bechgaard and J. M. Fabre, *J. Phys. (Paris) Colloq. C3*, 1983, **44**, 969–975.
41 V. Ilakovac, S. Ravy, J. P. Pouget, C. Lenoir, K. Boubekeur, P. Batail, S. Dolanski Babic, N. Biskup, B. Korin-Hamzic, S. Tomic and C. Bourbonnais, *Phys. Rev. B*, 1994, **50**, 7136–7139.

42 P. Auban-Senzier, C. Lenoir, P. Batail, D. Jérome and S. Tomic, *Eur. Phys. J. B*, 1999, **7**, 529–532.
43 K. Mortensen and E. M. Engler, *Phys. Rev. B*, 1984, **29**, 842–850.
44 (*a*) T. Naito, A. Miyamoti, H. Kobayashi, R. Kato and A. Kobayashi, *Chem. Lett.*, 1992, 119–122; (*b*) T. Naito, K. Bun, A. Miyamoto, H. Kobayashi, H. Sawa, R. Kato and A. Kobayashi, *Synth. Met.*, 1993, **56**, 2234–2240.
45 J. Sasaki, A. Kawamoto and K. Kumagai, *Synth. Met.*, 2003, **137**, 1249–1250.
46 T. Murata, X.-F. Shao, Y. Nakano, H. Yamochi, M. Uruichi, K. Yakushi, G. Saito and K. Tanaka, *Chem. Mater.*, 2010, **22**, 3121–3132.
47 M. J. Matos, V. Gama, G. Bonfait and R. T. Henriques, *Synth. Met.*, 1993, **55-57**, 1858–1863.
48 M. J. Matos, M. Almeida, L. Alcacer and R. T. Henriques, *Synth. Met.*, 1997, **86**, 2089–2090.
49 M. Matos, G. Bonfait, I. C. Santos, M. L. Afonso, R. T. Henriques and M. Almeida, *Magnetochemistry*, 2017, **3**(22), 1–13.
50 K. Mebrouk, W. Kaddour, P. Auban-Senzier, C. Pasquier, O. Jeannin, F. Camerel and M. Fourmigué, *Inorg. Chem.*, 2015, **54**, 7454–7460.
51 B. Zhou, M. Shimamura, E. Fujiwara, A. Kobayashi, T. Higashi, E. Nishibori, M. Sakata, H. B. Cui, K. Takahashi and H. Kobayashi, *J. Am. Chem. Soc.*, 2006, **128**, 3872–3873.
52 Y. Idobata, B. Zhou, A. Kobayashi and H. Kobayashi, *J. Am. Chem. Soc.*, 2012, **134**, 871–874.
53 S. K. Pal, P. Bag, M. E. Itkis, F. S. Tham and R. C. Haddon, *J. Am. Chem. Soc.*, 2014, **136**, 14738–14741.
54 P. Bag, M. E. Itkis, D. Stekovic, S. K. Pal, F. S. Tham and R. C. Haddon, *J. Am. Chem. Soc.*, 2015, **137**, 10000–10008.
55 G.-J. Yuan, H. Yang, S.-X. Liu, J.-L. Liua and X. M. Ren, *Dalton Trans.*, 2014, **43**, 11908–11914.
56 X. M. Ren, T. Akutagawa, S. Noro, S. Nishihara, T. Nakamura, Y. Yoshida and K. Inoue, *J. Phys. Chem. B*, 2006, **110**, 7671–7677.
57 A. Fukaya and R. Kato, *J. Phys. Soc. Jpn.*, 2008, **77**, 094710.
58 R. Kato, H. Sawa, S. Aonuma, M. Tamura, M. Kinoshita and H. Kobayashi, *Solid State Commun.*, 1993, **85**, 831–835.
59 A. Kobayashi, R. Kato and H. Kobayashi, *Chem. Lett.*, 1989, 1843–1846.
60 Y. Nishio, K. Kajita, W. Sasaki, R. Kato, A. Kobayashi and H. Kobayashi, *Solid State Commun.*, 1992, **81**, 473–476.
61 S. Hünig, M. Kemmer, H. Meixner, K. Sinzger, H. Wenner, T. Bauer, E. Tillmanns, F. R. Lux, M. Hollstein, H.-G. Groß, U. Langohr, H.-P. Werner, J. U. von Schütz and H. C. Wolf, *Eur. J. Inorg. Chem.*, 1999, 899–916.
62 P. Erk, S. Hünig, H. Meixner, H.-J. Gross, U. Langohr, H.-P. Werner, J. U. von Schütz and H. C. Wolf, *Angew. Chem., Int. Ed. Engl.*, 1989, 1245–1246.
63 (*a*) A. A. Zakhidov, K. Yakushi, K. Imaeda, H. Inokuchi, K. Kikuchi, S. Suzuki, I. Ikemoto and Y. Achiba, *Mol. Cryst. Liq. Cryst.*, 1992, **218**, 299–306; (*b*) A. A. Zakhidov, K. Imaeda, A. Ugawa, K. Yakushi, H. Inokuchi, Z. Iqbal, R. H. Baughman, B. L. Ramakrishna and Y. Achiba, *Phys. C*, 1991, **185–189**, 411–412.
64 (*a*) K. Tanaka, K. Yoshizawa, T. Sato, T. Yamabe, K. Okahara and A. A. Zakhidov, *Solid State Commun.*, 1993, **87**, 1055–1059; (*b*) K. Tanaka, T. Sato, T. Yamabe, K. Yoshizawa, K. Okahara and A. A. Zakhidov, *Phys. Rev. B*, 1995, **51**, 990–995.
65 K. Hiraki and K. Kanoda, *Synth. Met.*, 1997, **86**, 2111–2112.
66 T. Yamamoto, H. Tajima, J. Yamaura, S. Aonuma and R. Kato, *J. Phys. Soc. Jpn.*, 1999, **68**, 1384–1391.
67 R. Kato, T. Fukunaga, H. M. Yamamoto, K. Ueda and H. B. Cui, *Phys. Status Solidi B*, 2012, **249**, 999–1003.
68 E. W. Reinheimer, A. Assaf, O. Jeannin, A. Benallouche, P.-T. Nguyen, C. Coulon and M. Fourmigué, *Phys. Status Solidi B*, 2012, **249**, 943–946.
69 S. Tomic, D. Jérome, D. Mailly, M. Ribault and K. Bechgaard, *J. Phys. Colloq. France C3*, 1983, **44**, 1075–1079.
70 S. Ravy, R. Moret, J.-P. Pouget and R. Comes, *Phys. B+C*, 1986, **143**, 542–546.
71 V. Ilakovac, S. Ravy, K. Boubekeur, C. Lenoir, P. Batail and J. P. Pouget, *Phys. Rev. B*, 1997, **56**, 13878–13887.
72 (*a*) N. Joo, P. Auban-Senzier, C. R. Pasquier, P. Monod, D. Jérome and K. Bechgaard, *Eur. Phys. J. B*, 2004, **40**, 43–48; (*b*) N. Joo, P. Auban-Senzier, C. R. Pasquier, D. Jérome and K. Bechgaard, *Europhys. Lett.*, 2005, **72**, 645–651.
73 T. Yamaguchi, *Synth. Met.*, 2001, **120**, 1005–1006.
74 (*a*) R. Laversanne, J. Amiell, C. Coulon, C. Garrigou-Lagrange and P. Delhaes, *Mol. Cryst. Liq. Cryst.*, 1985, **119**, 317–320; (*b*) R. Laversanne, C. Coulon, B. Gallois, J. P. Pouget and R. Moret, *J. Phys. France Lett.*, 1984, **45**, L393–L399; (*c*) R. Laversanne, J. Amiell and C. Coulon, *Mol. Cryst. Liq. Cryst.*, 1986, **137**, 169–178.
75 F. Iwase, K. Sugiura, K. Furukawa and T. Nakamura, *Phys. Rev. B*, 2010, **81**, 245126.
76 M. Allain, C. Mézière, P. Auban-Senzier and N. Avarvari, *Crystals*, 2021, **11**, 386.
77 M. Tokumoto, H. Anzai, K. Murata, K. Kajimura and T. Ishiguro, *Synth. Met.*, 1988, **27**, A251–A256.
78 H. Anzai, M. Tokumoto, K. Takahashi and T. Ishiguro, *J. Cryst. Growth*, 1988, **91**, 225–228.
79 H. Kobayashi, R. Kato, A. Kobayashi, T. Mori and H. Inokuchi, *Solid State Commun.*, 1986, **60**, 473–480.
80 E. Amberger, H. Fuchs and K. Polborn, *Synth. Met.*, 1987, **19**, 605–610.
81 H. Kobayashi, R. Kato, A. Kobayashi, Y. Nishio, K. Kajita and W. Sasaki, *Chem. Lett.*, 1986, 789–792.
82 M. Fettouhi, L. Ouahab, D. Grandjean, L. Ducasse, J. Amiell, R. Canet and P. Delhaes, *Chem. Mater.*, 1995, **7**, 461–471.
83 (*a*) V. A. Bondarenko, Yu. V. Sushko, V. I. Barchuk, V. S. Yefanov, V. V. Dyakin, M. A. Tanatar, N. D. Kushch and E. B. Yagubskii, *Synth. Met.*, 1993, **56**, 2386–2390; (*b*) Yu. V. Sushko, K. Andres, N. D. Kusch and E. B. Yagubskii, *Solid State Commun.*, 1993, **87**, 589–592; (*c*) H. Posselt, H. Müller, K. Andres, Yu. V. Sushko and G. Saito, *Synth. Met.*, 1995, **70**, 917–918.
84 D. Faltermeier, J. Barz, M. Dumm, M. Dressel, N. Drichko, B. Petrov, V. Semkin, R. Vlasova, C. Mézière and P. Batail, *Phys. Rev. B*, 2007, **76**, 165113.

85 S. Yasin, M. Dumm, B. Salameh, P. Batail, C. Mézière and M. Dressel, *Eur. Phys. J. B*, 2011, **79**, 383–390.
86 H. Mori, T. Okano, S. Tanaka, M. Tamura, Y. Nishio, K. Kajita and T. Mori, *J. Phys. Soc. Jpn.*, 2000, **69**, 1751–1756.
87 H. Mori, M. Kamiya, M. Haemori, H. Suzuki, S. Tanaka, Y. Nishio, K. Kajita and H. Moriyama, *J. Am. Chem. Soc.*, 2002, **124**, 1251–1260.
88 A. D. Garlach, J. L. Musfeldt, J. M. Pigos, B. R. Jones, I. Olejniczak, A. Graja, M.-H. Whangbo, J. A. Schlueter, U. Geiser, R. W. Winter and G. L. Gard, *Chem. Mater.*, 2002, **14**, 2969–2976.
89 H. Tanaka, A. Kobayashi, T. Saito, K. Kawano, T. Naito and H. Kobayashi, *Adv. Mater.*, 1996, **8**, 812–815.
90 H. Akutsu, K. Kato, E. Ojima, H. Kobayashi, H. Tanaka, A. Kobayashi and P. Cassoux, *Phys. Rev. B*, 1998, **58**, 9294–9302.
91 H. Kobayashi, H. Akutsu, E. Arai, H. Tanaka and A. Kobayashi, *Phys. Rev. B*, 1997, **56**, R8526.
92 H. Kobayashi, A. Sato, E. Arai, H. Akutsu, A. Kobayashi and P. Cassoux, *J. Am. Chem. Soc.*, 1997, **119**, 12392–12393.
93 S. Uji, C. Terakura, T. Terashima, T. Yakabe, Y. Terai, M. Tokumoto, A. Kobayashi, F. Sakai, H. Tanaka and H. Kobayashi, *Phys. Rev. B*, 2002, **65**, 113101.
94 S. Uji, T. Terashima, C. Terakura, T. Yakabe, Y. Terai, S. Yasuzuka, Y. Imanaka, M. Tokumoto, A. Kobayashi, F. Sakai, H. Tanaka, H. Kobayashi, L. Balicas and J. S. Brooks, *J. Phys. Chem. Jpn.*, 2003, **72**, 369–373.
95 G. Kawaguchi, M. Maesato, T. Komatsu, T. Imakubo, A. Kiswandhi, D. Graf and H. Kitagawa, *Chem. Mater.*, 2016, **28**, 7276–7286.
96 M. Katsuhara, M. Aragaki, T. Mori, Y. Misaki and K. Tanaka, *Chem. Mater.*, 2000, **12**, 3186–3191.
97 M. Katsuhara, M. Aragaki, S. Kimura, T. Mori, Y. Misaki and K. Tanaka, *J. Mater. Chem.*, 2001, **11**, 2125–2130.
98 M. Katsuhara, S. Kimura, T. Mori, Y. Misaki and K. Tanaka, *Chem. Mater.*, 2002, **14**, 458–462.
99 T. Devic, M. Evain, Y. Moëlo, E. Canadell, P. Auban-Senzier, M. Fourmigué and P. Batail, *J. Am. Chem. Soc.*, 2003, **125**, 3295–3301.
100 P. Batail, K. Boubekeur, M. Fourmigué and J.-C. P. Gabriel, *Chem. Mater.*, 1998, **10**, 3005–3015.
101 A. Kitaigorodskii, *Mixed crystals*, Springer Verlag, Berlin, 1984.
102 K. Sarsuns, A. Berzins and T. Rekis, *Cryst. Growth Des.*, 2020, **20**, 7997–8004.
103 J. E. Eldridge, C. C. Homes, J. M. Williams, A. M. Kini and H. H. Wang, *Spectrochim. Acta, Part A*, 1995, **51**, 947–960.
104 E. Barthel, G. Quirion, P. Wzietek, D. Jérome, J. B. Christensen, M. Jørgensen and K. Bechgaard, *Europhys. Lett.*, 1993, **21**, 87–92.
105 M. Yamashita, A. Kawamoto and K. Kumagai, *Synth. Met.*, 2003, **133–134**, 125–127.
106 G. E. Pake, *J. Chem. Phys.*, 1948, **16**, 327–336.
107 A. Kawamoto, K. Miyagawa and K. Kanoda, *Phys. Rev. B*, 1997, **55**, 14140–14143.
108 B. R. McGarvey, M. J. Taylor and D. G. Tuck, *Inorg. Chem.*, 1981, **20**, 2010–2013.
109 R. Kirmse, J. Stach, W. Dietzsch, G. Steimecke and E. Hoyer, *Inorg. Chem.*, 1980, **19**, 2679–2685.
110 J. Stach, R. Kirmse, W. Dietzsch, R. M. Olk and E. Hoyer, *Inorg. Chem.*, 1984, **23**, 4779–4780.
111 R. Kumai, A. Asamitsu and Y. Tokura, *J. Am. Chem. Soc.*, 1998, **120**, 8263–8264.
112 R. Kato, *Bull. Chem. Soc. Jpn.*, 2014, **87**, 355–374.
113 J.-P. Pouget, P. Foury-Leylekian and M. Almeida, *Magnetochemistry*, 2017, **3**, 13.
114 V. Jaccarino and M. Peter, *Phys. Rev. Lett.*, 1962, **9**, 290–292.

